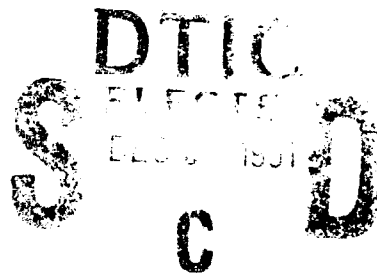


AD-A242 937



2

✓
NAVAL POSTGRADUATE SCHOOL
Monterey, California



THESIS

MICROSTRUCTURE AND MECHANICAL
PROPERTIES OF HSLA-100 STEEL

by

Victor R. Mattes

December, 1990

Thesis Advisor:

Alan G. Fox

Approved for public release; distribution is unlimited.

91-17045



91 12 4 037

Unclassified

security classification of this page

REPORT DOCUMENTATION PAGE

1a Report Security Classification Unclassified		1b Restrictive Markings	
2a Security Classification Authority		3 Distribution Availability of Report Approved for public release; distribution is unlimited.	
2b Declassification Downgrading Schedule		5 Monitoring Organization Report Number(s)	
4 Performing Organization Report Number(s)		6a Name of Performing Organization Naval Postgraduate School	
6b Office Symbol (if applicable) 34		7a Name of Monitoring Organization Naval Postgraduate School	
6c Address (city, state, and ZIP code) Monterey, CA 93943-5000		7b Address (city, state, and ZIP code) Monterey, CA 93943-5000	
8a Name of Funding Sponsoring Organization		8b Office Symbol (if applicable)	
8c Address (city, state, and ZIP code)		9 Procurement Instrument Identification Number	
		10 Source of Funding Numbers Program Element No Project No Task No Work Unit Accession No	
11 Title (include security classification) MICROSTRUCTURE AND MECHANICAL PROPERTIES OF HSLA-100 STEEL (Unclassified)			
12 Personal Author(s) Victor R. Mattes			
13a Type of Report Master's Thesis		13b Time Covered From To	14 Date of Report (year, month, day) December 1990
15 Page Count 80			

16 Supplementary Notation The views expressed in this thesis are those of the author and do not reflect the official policy or position of the Department of Defense or the U.S. Government.

17 Cosati Codes			18 Subject Terms (continue on reverse if necessary and identify by block number) HSLA-100, mechanical properties, copper precipitation, carbide
Field	Group	Subgroup	

19 Abstract (continue on reverse if necessary and identify by block number)

Light microscopy, scanning electron microscopy, and transmission electron microscopy were employed to examine the microstructural basis for the mechanical properties of as-quenched and tempered HSLA-100 steel. Examination of the alloy revealed granular bainite with martensite and retained austenite in the as-quenched state which upon aging at temperatures below the lower transformation temperature, 677°C, formed tempered bainite with precipitates of copper and carbides. These results indicate the strength and toughness of HSLA-100 steel aged below 677°C is based primarily on the fine prior austenite grain size and classic copper precipitation behavior but also on the bainitic dislocation substructure and carbides. After tempering at 677°C, HSLA-100 steel has a dual-phase microstructure consisting of bainitic ferrite laths, fine ferrite grain clusters and martensite with precipitates of carbides and overaged copper. The results indicate the yield strength of the overaged alloy is based on the fine ferrite grain and bainite lath sizes, the fine carbide distribution and elastic moduli strengthening while the toughness is the result of the high-angle ferrite grain boundaries, the fine intralath carbides and the ductile overaged copper precipitates.

20 Distribution Availability of Abstract <input checked="" type="checkbox"/> unclassified unlimited <input type="checkbox"/> same as report <input type="checkbox"/> DTIC users			21 Abstract Security Classification Unclassified
22a Name of Responsible Individual Alan G. Fox		22b Telephone (include Area code) (408) 646-2142	22c Office Symbol MEFx

DD FORM 1473 91 MAR

83 APR edition may be used until exhausted
All other editions are obsolete

security classification of this page

Unclassified

Approved for public release; distribution is unlimited.

Microstructure and Mechanical
Properties of HSLA-100 Steel

by

Victor R. Mattes
Lieutenant, United States Navy
B.S.M.E., Marquette University, 1982

Approved for	Distribution
Public Release	Universities
DTIC Type	Universities
Document Type	Classification
Information	
By	Classification
Dist	Specified

A-1

Submitted in partial fulfillment of the
requirements for the degrees of

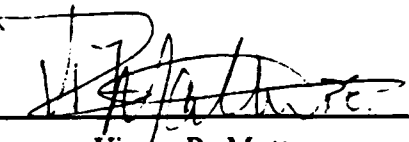
MASTER OF SCIENCE IN MECHANICAL ENGINEERING
and
MECHANICAL ENGINEER

from the

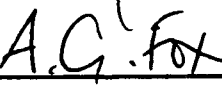
NAVAL POSTGRADUATE SCHOOL

December 1990

Author:


Victor R. Mattes

Approved by:


Alan G. Fox, Thesis Advisor


A.J. Healey, Chairman,
Department of Mechanical Engineering


Gordon E. Schacher
Dean of Science and Engineering

ABSTRACT

Light microscopy, scanning electron microscopy, and transmission electron microscopy were employed to examine the microstructural basis for the mechanical properties of as-quenched and tempered HSLA-100 steel. Examination of the alloy revealed granular bainite with martensite and retained austenite in the as-quenched state which upon aging at temperatures below the lower transformation temperature, 677°C, formed tempered bainite with precipitates of copper and carbides. These results indicate the strength and toughness of HSLA-100 steel aged below 677°C is based primarily on the fine prior austenite grain size and classic copper precipitation behavior but also on the bainitic dislocation substructure and carbides. After tempering at 677°C, HSLA-100 steel has a dual-phase microstructure consisting of bainitic ferrite laths, fine ferrite grain clusters and martensite with precipitates of carbides and overaged copper. The results indicate the yield strength of the overaged alloy is based on the fine ferrite grain and bainite lath sizes, the fine carbide distribution and elastic moduli strengthening while the toughness is the result of the high-angle ferrite grain boundaries, the fine intralath carbides and the ductile overaged copper precipitates.

TABLE OF CONTENTS

I. INTRODUCTION	1
II. BACKGROUND	3
A. METALLURGICAL DESIGN OF HSLA STEELS	3
B. METALLURGICAL DESIGN OF HSLA-100 STEEL	3
C. MOLTEN METAL PROCESSING	9
D. THERMO-MECHANICAL PROCESSING OF HSLA-100 STEEL	10
E. THE AGING BEHAVIOR OF COPPER	12
F. MICROSTRUCTURE OF HSLA-100 STEEL	15
G. LOW-CARBON BAINITE STRENGTH AND TOUGHNESS PROPER- TIES	17
1. Upper Bainite	18
2. Lower Bainite	18
3. Strengthening Mechanisms	18
4. Toughness Properties	20
H. MECHANICAL PROPERTIES OF HSLA-100 STEEL	22
I. SCOPE OF PRESENT WORK	25
III. EXPERIMENTAL PROCEDURE	26
A. MATERIAL	26
B. MECHANICAL PROPERTIES	26
C. MICROSCOPY	27
1. Optical Microscopy	27
2. Scanning Electron Microscopy	27
3. Transmission Electron Microscopy	27
IV. EXPERIMENTAL RESULTS	29
A. MECHANICAL BEHAVIOR	29
B. MICROSTRUCTURE	35
1. As-quenched HSLA-100 Steel	35
2. 454°C Aged HSLA-100 Steel	40

3. 566°C Aged HSLA-100 Steel	46
4. 677°C Aged HSLA-100 Steel	50
V. DISCUSSION	61
VI. CONCLUSIONS	64
VII. RECOMMENDATIONS FOR FUTURE RESEARCH	65
LIST OF REFERENCES	66
INITIAL DISTRIBUTION LIST	69

LIST OF TABLES

Table 1. ROLE OF MAJOR ALLOYING ELEMENTS IN STEEL ALLOYS . . .	4
Table 2. HSLA-100 STEEL MIL-S-24654A COMPOSITION	5
Table 3. SOLID SOLUTION ALLOYING ELEMENTS AND MECHANICAL PROPERTIES	5
Table 4. HSLA-100 STEEL STRENGTH AND TOUGHNESS REQUIREMENTS	24
Table 5. HSLA-100 STEEL LOT GQH CHEMICAL COMPOSITION	26

LIST OF FIGURES

Figure 1. Graville Diagram	6
Figure 2. HSLA-100 Steel Continuous Cooling Transformation Diagram	8
Figure 3. Fe-Cu Phase Diagram	13
Figure 4. High Strength Bainite Strength Components	20
Figure 5. Bainitic Steel Tempering and DBTT	21
Figure 6. Tempered Bainite Steel Yield Stress and DBTT	21
Figure 7. HSLA-100 Steel Yield Strength versus Aging Temperature	22
Figure 8. HSLA-100 Steel Charpy V-notch Energy versus Aging Temperature ..	23
Figure 9. HSLA-100 Steel Charpy V-notch Energy Transition (1 in. thick)	24
Figure 10. 566°C Aged HSLA-100 Steel Back-Scattered SEM Micrograph	27
Figure 11. HSLA-100 Steel Lot GQH 0.2% Yield Strength	29
Figure 12. HSLA-100 Steel Lot GQH Tensile Strength	30
Figure 13. HSLA-100 Steel Lot GQH Impact Energy at -84°C	31
Figure 14. HSLA-100 Steel Lot GQH DBTT	31
Figure 15. HSLA-100 Steel Lot GQH Ductility	32
Figure 16. HSLA-100 Steel Lot GQH Bainite Parameters	34
Figure 17. TEM Image of As-quenched HSLA-100 Steel Lath Structure	35
Figure 18. Micrographs of As-quenched HSLA-100 Steel Grain Structure	36
Figure 19. TEM Images of As-quenched HSLA-100 Steel Retained Austenite	37
Figure 20. TEM Images of Martensite in As-quenched HSLA-100 Steel	38
Figure 21. As-quenched HSLA-100 Steel SADP	39
Figure 22. TEM Bright Field Image of Retained Austenite in As-quenched HSLA-100 Steel	39
Figure 23. TEM Dark Field Image of Retained Austenite in As-quenched HSLA-100 Steel	40
Figure 24. Micrographs of 454°C Aged HSLA-100 Steel Grain Structure	41
Figure 25. TEM Image of 454°C Aged HSLA-100 Steel Lath Structure	42
Figure 26. TEM Image of 454°C Aged HSLA-100 Steel Copper Coherency Strain Field	42
Figure 27. TEM Image of 454°C Aged HSLA-100 Steel Copper Coherency Strain Field	43

Figure 28. 454°C Aged HSLA-100 Steel SADP	43
Figure 29. TEM Dark Field Image of 454°C Aged HSLA-100 Steel Intralath Carbides	44
Figure 30. TEM Image of Martensite in 454°C Aged HSLA-100 Steel	44
Figure 31. TEM Images of 454°C Aged HSLA-100 Steel Interlath Carbides	45
Figure 32. Micrographs of 566°C Aged HSLA-100 Steel Grain Structure	47
Figure 33. TEM Image of 566°C Aged HSLA-100 Steel Lath Structure	48
Figure 34. 566°C Aged HSLA-100 Steel SADP	48
Figure 35. TEM Bright Field Image of Copper Precipitates in 454°C Aged HSLA-100 Steel	49
Figure 36. TEM Dark Field Image of Copper Precipitates in 454°C Aged HSLA-100 Steel	49
Figure 37. Micrographs of 677°C Aged HSLA-100 Steel Grain Structure	52
Figure 38. TEM Images of Bainite Lath and Ferrite Grain Structure in 677°C Aged HSLA-100 Steel	53
Figure 39. TEM Image of 677°C Aged HSLA-100 Steel Lath Structure	54
Figure 40. 677°C Aged HSLA 100 Steel SADP	54
Figure 41. TEM Images of 677°C Aged HSLA-100 Steel Interlath and Intralath Carbides	55
Figure 42. 677°C Aged HSLA-100 Steel Carbide EDX Spectra	56
Figure 43. X-ray Mapping of 677°C Aged HSLA-100 Steel	57
Figure 44. TEM Image of Lath Boundary Copper Precipitates in 677°C Aged HSLA-100 Steel	58
Figure 45. TEM Images of Interlath Copper Precipitates in 677°C Aged HSLA-100 Steel	59
Figure 46. TEM Image of Copper Precipitates on Dislocations in 677°C Aged HSLA-100 Steel	60

ACKNOWLEDGMENTS

I would like to thank Professor Alan G. Fox for his technical guidance in the pursuit of this thesis. I would also like to thank Chuck Echer, of the National Center for Electron Microscopy, and Elisabeth Grayson for their technical support. Finally, I would also like to thank Dr. M.G. Vassilaros and Stephanie Mickalac of David Taylor Research Center for providing the HSLA-100 steel samples and the associated mechanical properties test data.

I. INTRODUCTION

The development of low carbon, copper bearing, precipitation strengthened high-strength, low-alloy (HSLA) plate steel has been a key element of the U.S. Navy's efforts to reduce shipbuilding costs. A significant portion of the fabrication costs of the HY-80 and HY-100 steels traditionally used in naval ship construction have been associated with the necessity for fabrication controls to avoid hydrogen-induced cold cracking in the heat affected zone [Ref. 1: p. 38]. These controls include preheat requirements, interpass temperature limits, controls on electrode preparation, storage and issue, heat input limits, weld sequencing requirements, weather protection, constraint reduction, welder training and qualification, and intensive inspection procedures [Ref. 2: p. 2].

The U.S. Navy selected ASTM A710 Grade A steel, designated HSLA-80 by the Navy, as the replacement for HY-80 steel. HSLA-80 steel was certified for use in surface ship structural construction following evaluation of its structural and welding properties [Ref. 3]. Significant reduction in hull fabrication costs were realized through the reduced requirements for process controls and inspections [Ref. 4: p. 64]. HSLA-80 steel is currently used as a primary structural steel in the construction of the Ticonderoga-class cruisers, the new Arleigh Burke-class destroyers, in some structures of the later Nimitz-class aircraft carriers and the Wasp-class amphibious assault ships [Ref. 2: p. 3].

Based on the success of the HSLA-80 steel program, the U.S. Navy expanded the HSLA steel program to develop a HSLA-100 steel as the replacement for the HY-100 steel being used in the advanced submarine non-pressure hull structural design and in surface ship topside construction for weight reduction [Ref. 4: p. 64]. Although HY-100 steel had excellent strength, toughness and resistance to seawater corrosion, it suffered from similar weld cracking problems as HY-80 steel and required extensive fabrication controls [Ref. 5: p. 2]. The large quantities of HY-100 steel required would have resulted in high fabrication and production costs due to the need for fabrication controls. [Ref. 5: p. 2]. The object of the HSLA-100 program was to develop an alloy steel that would meet or exceed the toughness and strength properties of HY-100 steel, be weldable without preheat requirements and use the same welding consumables and processes as used by HY-100 steel [Ref. 4: p. 64]. HSLA-100 steel was developed by the AMAX Materials Research Center, under contract from the David Taylor Research Center (DTRC), as a low-carbon, copper precipitation strengthened steel similar to

HSLA-80 steel but based on different metallurgical principles [Ref. 2: p. 3]. HSLA-80 steel was used as the base metal to develop HSLA-100 steel from in order to save time and money [Ref. 2: p. 2]. Certification of HSLA-100 steel was completed in 1989 and the first major order was placed for use in the construction of the Nimitz-class aircraft carrier, USS John C. Stennis (CVN-74) [Ref. 4 : p. 64].

Fracture studies of HSLA-80 steel showed that coarse-grained polygonal ferrite and accumulated second phase products were detrimental to the low-temperature fracture resistance and, therefore, a uniformly fine grain size with a wider distribution of the small carbides would reduce the fracture transition temperature. The key to the HSLA-100 alloy design was the requirement to produce a homogeneous microstructure which dispersed the secondary transformation products. The goal of the HSLA-100 steel metallurgical design was a bainitic matrix to take advantage of the excellent combination of the strength and toughness properties normally associated with tempered bainite. The object of this thesis is to investigate the microstructural basis for the strength and toughness properties of HSLA-100 steel, in particular the overaged steels where anomalously high fracture toughnesses have been observed. [Ref. 2: p. 9-10]

II. BACKGROUND

A. METALLURGICAL DESIGN OF HSLA STEELS

High-strength, low-alloy (HSLA) steels constitute a successful metallurgical innovation in which alloying additions and thermomechanical processing have been brought together effectively to attain improved combinations of engineering properties through microstructural control [Ref. 6: p.61]. The physical metallurgy principles in HSLA steels include inclusion morphology, carbonitride solubility, grain refinement, precipitation hardening and substructure strengthening [Ref. 7: p. 581]. While substantial improvements have been made in the thermomechanical processing of steels, the secret of the success of HSLA steels is in the microalloying where the addition of small amounts of elements such as niobium, titanium or vanadium can make all the difference. Table 1 [Ref. 8: p. 376] gives a short list of such elements and their contribution to steels.

Varying the alloy content modifies the microstructure by altering the continuous cooling transformation (CCT) behavior, in particular the location of the proeutectoid ferrite C-curve, and allowing the formation of ferrite-pearlite, ferrite-bainite, tempered martensite or bainitic microstructures. Although precipitation hardening and substructural changes due to warm rolling of austenite-ferrite mixtures can contribute to the strengthening of HSLA steels, the key feature of the ultimate microstructure is the fine prior austenite grain size, the result of the alloying and modifications of the CCT curve, which provides the favorable balance between strength and toughness in as-quenched HSLA steels [Ref. 6: p. 61].

B. METALLURGICAL DESIGN OF HSLA-100 STEEL

HSLA-100 steel is a highly weldable, copper precipitation strengthened, low carbon, 690 MPa yield strength steel (See Table 2 for MILSPEC MIL-S-24645A chemical composition). The HSLA-100 steel metallurgical design derived by the AMAX Materials Research Center under contract from DTRC was a modification of the previously certified HSLA-80 steel in order to reduce the certification time necessary to allow its use for

Table 1. ROLE OF MAJOR ALLOYING ELEMENTS IN STEEL ALLOYS

Element	Function
C	Extremely potent hardenability agent and solid solution strengthener; carbides also provide strengthening but serve to nucleate cracks
Ni	Extremely potent toughening agent; lowers ductile-to-brittle transition temperature (DBTT); hardenability agent; austenite stabilizer
Cr	Provides corrosion resistance in stainless steels; hardenability agent in quenched and tempered steels; solid solution strengthener; strong carbide former
Mo	Hardenability agent in quenched and tempered steels; suppresses temper embrittlement; solid solution strengthener; strong carbide former
Si	Deoxidizer; increases σ_y and DBTT when found in solid solution
Mn	Deoxidizer; forms MnS, which precludes hot cracking caused by grain-boundary melting of FeS films; lowers DBTT; hardenability agent
Co	Used in maraging steels to enhance martensite formation and precipitation hardening kinetics
Ti	Used in maraging steels for precipitation hardening; carbide and nitride former
V	Strong carbide and nitride former
Al	Strong deoxidizer; forms AlN, which pins grain boundaries and keeps ferrite grain size small. AlN formation also serves to remove N from solid solution, thereby lowering lattice resistance to dislocation motion and lowering DBTT
Nb	Strong carbide and nitride former

naval ship construction. The DTRC contract stipulated that [Ref. 5: p. 2]:

the new steel be copper precipitation strengthened, contain columbium (niobium) for grain-size control, have maximum carbon, sulfur, and phosphorus contents of 0.07%, 0.008%, and 0.010%, respectively, and also contain at least all of the hardenability elements Mn, Ni, Cr, and Mo that are present in HSLA-80. It was also required that the steel be solution treated, quenched, and aged. . .

The design of HSLA steels relies on the contribution of several strengthening mechanisms including grain refinement, precipitation hardening, solid solution strengthening and dislocation substructures resulting from phase transformations or deformation processes [Ref. 5: p. 2, Ref. 9: p. 64-69]. The Navy requirement that the new steel be low carbon, copper precipitation strengthened and 690 MPa yield strength

Table 2. HSLA-100 STEEL MIL-S-24654A COMPOSITION

C	Mn	P	S	Si
0.06	0.75-1.05	0.020	0.006	0.40
Ni	Cr	Mo	Cu	Nb
3.35-3.65	0.45-0.75	0.55-0.65	1.45-1.75	0.02-0.06

eliminated all strengthening mechanisms relying on carbon addition and deformation induced substructures [Ref. 5: p. 3]. The benefits of the low carbon content are improved toughness and weldability although the solid solution strengthening potential lost is substantial (Table 3, from Ref. 9: p. 70). Additionally, the solid solution strengthening potentials of the remaining alloying elements of HSLA-100 steel are minimal as seen in Table 3, effectively eliminating solid solution strengthening as a major strengthening mechanism in HSLA-100 steel.

Table 3. SOLID SOLUTION ALLOYING ELEMENTS AND MECHANICAL PROPERTIES

Element	Change per 1 wt % alloying element		
	Yield Stress (MPa)	Tensile Strength (MPa)	Impact Transition Temperature (°C)
C	+ 4600	+ 6800	----
N	+ 4600	+ 6800	+ 700
P	+ 670	+ 670	+ 400
Sn	+ 140	---	+ 150
Si	+ 85	+ 85	+ 44
Cu	+ 39	+ 9	---
Mn	+ 32	+ 28	0
Mo	+ 11	+ 45	---
Ni	0	+ 9	---
Cr	-30	-28	---
Al	0	0	+ 75

The impact of the low carbon content on weldability can best be seen on the Graville diagram, Figure 1, [Ref. 2: p. 16]. The Graville diagram uses the carbon and the carbon equivalent content to establish three regions which attempt to predict the ease with which a steel can be welded. The traditional construction steels, HY-80 and HY-100, lie in zone III which is difficult to weld and require extensive and expensive welding procedures. Construction experience with HY-80 and HY-100 steels have given credence to this prediction. HSLA-100 steel and its parent HSLA-80 steel have such low carbon content that they fall into zone I which predicts easily weldable steels.

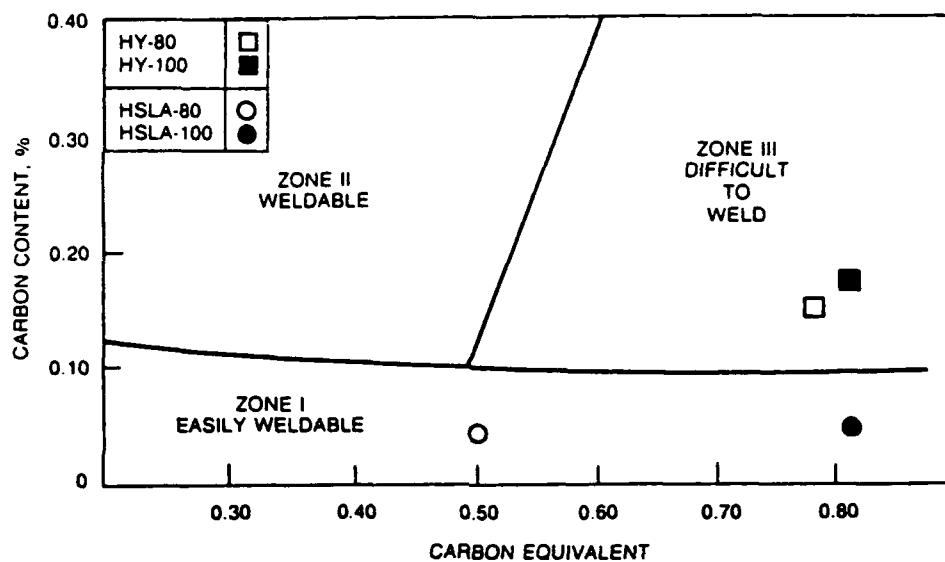


Figure 1. Graville Diagram

The strength of HSLA-100 steel is due primarily to the fine-grained bainitic micro-structure, which evolves from the refined prior austenite grain structure [Ref. 5: p. 4]. The refined prior austenite grain structure, the result of the thermomechanical processing, is enhanced by the addition of small amounts of niobium. The niobium combines with carbon and nitrogen in austenite to form niobium carbonitride ($\text{Nb}(\text{C},\text{N})$) precipitates. The precipitation of $\text{Nb}(\text{C},\text{N})$ is coupled with the recrystallization of the austenite during the hot rolling process. Substructural features in the deformed, unrecrystallized austenite provide the nucleation sites for the carbonitride precipitation while the carbonitride precipitates, if of sufficient volume fraction and fineness, tend to pin the substructure and inhibit the austenite recrystallization [Ref. 6: p. 64]. The result of these

interactions during the hot rolling is a pancaked austenite microstructure. The thickness of the austenite grains just prior to cooling is the key microstructural feature influencing the grain size of the transformed microstructure [Ref. 6: p. 64]. Some niobium carbonitrides may also precipitate during and after the transformation to provide additional refinement of the grain size and some precipitation hardening. The refined grain structure strengthens and toughens the alloy and lowers the ductile-to-brittle transition temperature.

The strengthening mechanisms remaining available for use in raising the yield strength of HSLA-100 steel from that provided by the grain-refined microstructure to the required 690 MPa were precipitation hardening and transformation induced dislocation substructures. The structural feature, aside from grain size, most affecting the as-quenched strength of low-carbon bainitic steels, such as HSLA-100 steel, is the density of the dislocation substructure produced by the transformation of austenite to bainite. The bainite transformation temperature is controlled by alloying elements as follows [Ref. 5: p. 8]:

$$B_s(^{\circ}C) = 830 - 270C - 90Mn - 37Ni - 70Cr - 83Mo \quad (1)$$

As the bainite transformation temperature is lowered either by alloying, as above, or by faster cooling, the dislocation density is increased and the strength raised. During any subsequent aging treatment, the dislocation density is affected by two competing reactions. The aging tempers the dislocation substructure by the annihilation and rearrangement of the dislocations, resulting in lower strength while precipitation of copper and carbides of niobium and molybdenum increase the strength. Careful selection of the alloy content is necessary to produce a steel with the desired mechanical properties. [Ref. 5: pp. 3-14]

The most prevalent element in HSLA-100 steel is nickel. Nickel was originally added to copper bearing steels to prevent the hot shortness associated with the welding of such alloys [Ref. 10: p. 260] but it also plays a beneficial role in improving the toughness and lowering the DBTT of HSLA steels through a mechanism which remains unclear [Ref. 8: p. 375].

The nickel, with the molybdenum, manganese, chromium and copper, acts as an austenite stabilizer by substantially increasing the hardenability of HSLA-100 steel through the shifting of the nose of the CCT diagram to the right (Figure 2 from Ref. 10) and lowering the B_s temperature as seen in equation (1). The shift in the CCT curve

to longer transformation times significantly increases the size of the austenite field and allows the formation of bainite with its high dislocation density at a more economically feasible cooling rate, a more uniform through thickness microstructure and an increased supersaturation of copper and other alloying elements in the quenched condition. This results in not only a stronger alloy but a tougher alloy through the reduction of the DBTT and the increased upper shelf impact energy [Ref. 4: p. 64]. The copper supersaturated matrix allows significant precipitation hardening during the subsequent aging heat treatment with increases in strength of up to 248 MPa for each 1% copper [Ref. 11: p. 23]. This strengthening effect is substantially greater than that possible through the use of copper as a solid solution strengthener, 39 MPa per 1% copper (from Table 3), and is the primary reason for the increased copper content of HSLA-100 steel over that of HSLA-80 steel [Ref. 11: p. 21]. The copper also improves weldability by reducing the hydrogen absorption through the formation of a stable protective surface [Ref. 12: p. 67.] and, in combination with the chromium, molybdenum, nickel and manganese, provides good corrosion resistance in seawater and the atmosphere [Ref. 11: pp. 111-116].

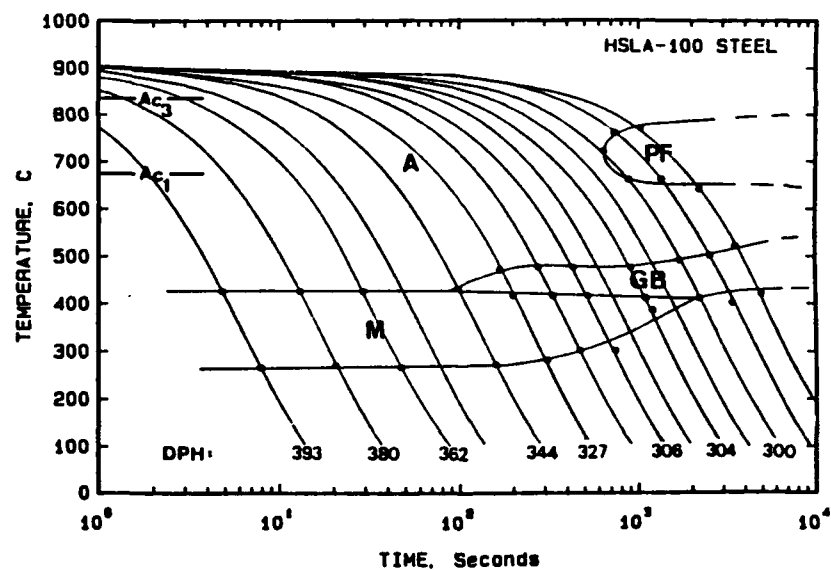


Figure 2. HSLA-100 Steel Continuous Cooling Transformation Diagram

C. MOLTEN METAL PROCESSING

The presence of certain elements, such as those listed in Table 1, in alloys will result in the development of optimum microstructures. However, elements such as sulfur and phosphorus serve no useful purpose in the alloy and can be detrimental to mechanical properties, in particular toughness. The goal of the processing of the steel while it is molten, in addition to forming a uniform melt, is to remove as many tramp and gaseous elements as possible. The steel is melted in an electric arc or basic oxygen furnace before being tapped into a ladle where aluminum (Al) is added and CaSi is argon-injected for tramp element and inclusion control. Argon stirring with a CaO-based cover slag is used to mix the hot metal in order to reduce the sulfur content and release the trapped gases [Ref. 13: p. 14]. The aluminum is added to the melt in order to deoxidize the melt and remove nitrogen from solid solution by the formation of AlN during solidification. Removal of the nitrogen lowers the lattice resistance to dislocation motion and the transition temperature. The AlN also pins austenite grain boundaries, helping to refine the prior austenite grain size. The CaSi is added for deoxidation, desulfurisation and inclusion shape control. The ladle is then capped and sealed and a vacuum established to remove as much of the remaining trapped gas before the melt is poured into a mold to form the ingot. [Ref. 8: p. 364-379]

A problem faced by not only HSLA steels but by all steels is the loss of ductility due to the presence of non-metallic second phase inclusions [Ref. 9: p. 81]. Sulfides, in addition to being the most predominant type of inclusions in steel, have the most detrimental effect on the ductility and toughness of a steel. The major deterioration occurs as the result of MnS inclusions becoming elongated into stringers during the hot-rolling process. When the steel is strained, voids nucleate around the MnS inclusions and grow and coalesce until ductile failure occurs. Al_2O_3 inclusions produce similar problems due to their brittleness and tendency to string out during hot work. Steel melts are Al-killed and argon-injected with CaSi to desulfurize and deoxidize the melt and to ensure the inclusions that do form are globular complex mixtures of Ca-S-Al-O and Ca(Mn)S vice the more deleterious MnS or Al_2O_3 . These complex inclusions are hard and extremely resistant to deformation at hot-rolling temperatures. Because of their low stress-concentration factors in the transverse direction, the spherical sulfides and oxides exhibit significantly less rapid void growth and coalescence than do the stringers. The non-deformed, spherical inclusion morphology provides for increased transverse and through-thickness ductility as well as improved toughness. [Ref. 9: p. 81-83, Ref. 7: p. 581]

D. THERMO-MECHANICAL PROCESSING OF HSLA-100 STEEL

HSLA-100 heats for use by the Navy (DTRC) are usually produced using conventional electric arc furnace techniques with vacuum degas and Al and argon-injected CaSi treatments [Ref. 4: p. 66]. Ingots are formed in bottom-flow molds and thermo-mechanically processed to plate thicknesses of 12.7 to 95.25mm. The thermo-mechanical treatment of the HSLA-100 steel ingots, in addition to attaining the proper plate thickness, plays a vital role in the production of the fine grained microstructure. The following discussion on the thermo-mechanical treatment of HSLA plate steels is a condensation of an excellent paper on this subject by Cohen and Hansen [Ref. 6].

The thermo-mechanical processing consists of four parts: slab reheating, hot rolling, transformation to bainite and precipitation strengthening. The slab reheating begins the evolution of the austenitic microstructure by dissolving the complex carbonitrides formed during the casting of the ingots. The carbonitrides which are dissolved and their constituent elements influence the austenite behavior during rolling or may precipitate later in the bainite in fine form to provide a strengthening effect.

In addition to controlling the amount of microalloying elements dissolved prior to rolling, the reheating temperature influences the austenite grain size. While it is advantageous to maximize the dissolution of the carbonitrides, it is also essential to avoid austenitic grain growth as much as possible. A fine, uniform, as-reheated austenitic grain size helps minimize the development of a duplex austenitic structure after rolling which will improve toughness. Control of the austenitic grain size is primarily the result of grain boundary pinning provided by the fine, second-phase particles which remain undissolved during reheating. Therefore, in slab reheating, a balance must be struck between dissolution of the carbonitrides and the austenitic grain growth.

The rolling process typically begins at temperatures just below the slab reheat temperature, in the range of 1100 to 1250°C. At these temperatures, each deformation step is usually followed by rapid recrystallization and grain growth. Repeated deformation steps will result in a refined austenite grain size. Still finer grain sizes are realized through the use of carbonitride forming elements such as niobium. During this process, the austenite recrystallization and carbonitride precipitation become coupled in the sense that one depends on the other. Substructural features in the deformed, unrecrystallized austenite provide the nucleation sites for carbonitride precipitation while the precipitated carbonitrides will tend to pin the substructure and inhibit recrystallization. These interactions make it possible to roll below a temperature where recrystallization does not occur between rolling passes and the plastically deformed austenite grains remain flat-

tened. The flattened, pancake-like morphology of the austenite grains is one goal of the hot rolling process as it is the thickness of the flattened grains that controls the grain size of the alloy following phase transformation.

The subsequent transformation of the refined austenite microstructure into a bainitic microstructure determines the final grain size and associated mechanical properties. The effects of the austenitic morphology and the transformation temperature range, as governed by the alloy content, rolling deformation and cooling rate, are of most importance. The transformation process for HSLA-100 steel consists of an austenization and quench for gages up to 31.75mm and a double austenization and quench for larger gages. The austenization serves the same purpose as slab reheating and carries with it the same concerns of carbonitride dissolution versus austenite grain growth and need for control of the austenitizing temperature. The double austenitization and quench provides additional grain refinement and minimizes the possibility of large isolated austenite grains [Ref. 13: p. 16]. Further control of the grain size is achieved by control of the reaction kinetics associated with the quench. This is accomplished through control of the bainite transformation temperature. As seen in equation (1), use of the proper amounts of certain alloying elements will lower the B_c . As the B_c is lowered, the number of bainite nucleation sites increases at the expense of the bainitic grain growth, resulting in a smaller grain size. The beneficial reaction kinetics are also achieved through modification of the CCT diagram by increasing the hardenability of the alloy and quenching.

The object of the quench is to produce a finely-grained microstructure which is supersaturated with the microalloying elements, in particular copper and niobium. Some precipitation of the carbonitrides may occur during the quench due to the greater solubility of the carbides and nitrides in austenite than in bainite. The carbonitrides form on a fine scale during the austenite to bainite transformation as their nucleation and growth depends on the diffusivity of the alloying elements in addition to that of carbon, resulting in an intimate association of the precipitating carbide or carbonitride and the migrating austenite-bainite interface [Ref. 14: p. 246].

To this point in the thermo-mechanical processing, the mechanical properties of the alloyed steel have been controlled by the steel's grain size. While the refined grain structure does provide the basis for the steel's strength and toughness, there is a practical limit to the grain size-based yield strength that can be achieved. To achieve higher strengths, classic precipitation strengthening is used. HSLA-100 steel is aged at various temperatures, dependent upon the plate thickness, in order to produce the optimum

combination of properties. The predominant precipitation strengthening element used in HSLA-100 steel is copper although some strengthening can result from the precipitation of niobium and molybdenum carbides.

E. THE AGING BEHAVIOR OF COPPER

The phase boundaries of the FeC system are modified by the presence of other alloying elements in a manner that can modify the transformation characteristics on cooling, the strength of the various phases present after cooling and the possibility of strengthening by subsequent heat treatments [Ref. 11: p. 5]. Copper, because of its low solubility in bainite, has such a capability and provides many benefits to low-carbon HSLA steels [Ref. 12: p.64]:

1. Increased strength through precipitation of ϵ -copper while retaining good toughness, weldability and formability.
2. Excellent corrosion resistance.
3. Production of bainitic acicular microstructures when used in conjunction with other microalloying elements.
4. High fatigue strength and resistance to fatigue crack growth.
5. Suppression of hydrogen induced cracking.

The disadvantage of the use of copper is the increased susceptibility of the alloy to hot shortness during welding but this can be prevented by the use of nickel in the alloying mixture.

Examination of the iron-rich portion of the Fe-Cu phase diagram illustrates the solubility of copper in iron (Figure 3, from Ref. 11: p. 8). The maximum solubility of copper in α -iron is 2.1% at 849°C and its decreasing solubility with decreasing temperature provides the opportunity for age hardening to used [Ref. 11 : p. 6]. The limited solubility of copper in α -iron minimizes the potential for solid solution strengthening of the matrix and, as a result, the addition of copper to HSLA steels is primarily to take advantage of the aging behavior of the copper supersaturated matrix.

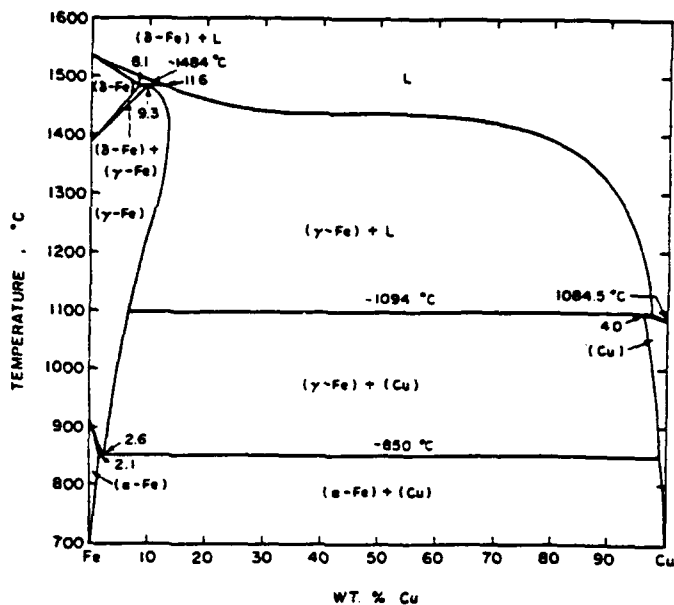


Figure 3. Fe-Cu Phase Diagram

Hornbogen showed that the precipitation of copper from ferrite occurs first with the uniform formation throughout the matrix of coherent BCC clusters which transform into incoherent FCC copper when they become large enough [Ref. 15: p. 1067]. The clustering process cannot be followed by transmission electron microscopy, x-ray diffraction or electron diffraction because of the similiar electron and x-ray scattering factors of the iron and copper atoms and of the small coherency strain. Hornbogen surmized that the clusters were spherical because of the similiar sizes of the iron and copper atoms and provided nucleation sites for the FCC phase [Ref. 16: p. 121].

Goodman, Brenner and Low, using field ion microscopy, observed that the coherent, copper-rich clusters formed in the ferrite during aging and grew by bulk diffusion. The BCC clusters contained less copper than the equilibrium ε -phase which eventually formed from them. The maximum strength occurred when the precipitates were still BCC at a diameter of 24Å and a copper content of about 50%. Additionally, they found that the number density of copper precipitates remained nearly constant until peak strength was reached and then decreased during overaging.[Refs. 17,18]

The size and distribution of the clusters becomes evident after the clusters transform to FCC as the loss of coherency makes them visible in the transmission electron microscope [Ref. 18: p. 121]. The transformation from BCC to FCC occurs when the clusters

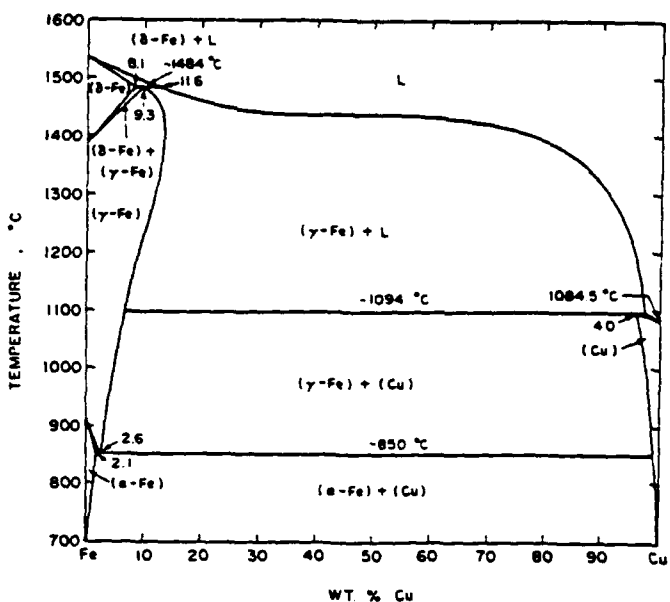


Figure 3. Fe-Cu Phase Diagram

Hornbogen showed that the precipitation of copper from ferrite occurs first with the uniform formation throughout the matrix of coherent BCC clusters which transform into incoherent FCC copper when they become large enough [Ref. 15: p. 1067]. The clustering process cannot be followed by transmission electron microscopy, x-ray diffraction or electron diffraction because of the similiar electron and x-ray scattering factors of the iron and copper atoms and of the small coherency strain. Hornbogen surmized that the clusters were spherical because of the similiar sizes of the iron and copper atoms and provided nucleation sites for the FCC phase [Ref. 16: p. 121].

Goodman, Brenner and Low, using field ion microscopy, observed that the coherent, copper-rich clusters formed in the ferrite during aging and grew by bulk diffusion. The BCC clusters contained less copper than the equilibrium ϵ -phase which eventually formed from them. The maximum strength occurred when the precipitates were still BCC at a diameter of 24Å and a copper content of about 50%. Additionally, they found that the number density of copper precipitates remained nearly constant until peak strength was reached and then decreased during overaging.[Refs. 17,18]

The size and distribution of the clusters becomes evident after the clusters transform to FCC as the loss of coherency makes them visible in the transmission electron microscope [Ref. 18: p. 121]. The transformation from BCC to FCC occurs when the clusters

strength increment. Russell and Brown offered the theory that the strengthening was due to the differences in the elastic moduli of the particle and the matrix [Ref. 21: p. 969]. They demonstrated that the strengthening of overaged copper particles could be accounted for through the interaction between matrix slip dislocations and second phase particles of lower elastic moduli than the matrix material without the work hardening or dislocation loops normally associated with Orowan hardening.

F. MICROSTRUCTURE OF HSLA-100 STEEL

Although HSLA-100 is a relatively new steel, several studies have been conducted investigating the nature of its microstructure. The object of this section is to review these studies and describe the current knowledge about the microstructure.

As stated earlier, HSLA-100 steel was designed by the AMAX Materials Research Center. To achieve the best combination of strength and toughness required by DTRC, it was decided that a 100% low-carbon bainitic microstructure was the best metallurgical approach. Optical and scanning electron microscope (SEM) micrographs of the laboratory plates exhibited the desired bainitic microstructure. Dispersed within the bainitic microstructure were high carbon microconstituents consisting of carbides and very small islands of martensite-austenite. [Ref. 5: p. 8-13]

Wilson et al [Ref. 10: p. 263-265], working at Lukens Steel Company's Coatesville Works and the Colorado School of Mines, found the dominant phase in thin and intermediate thickness plates of 0.06%C HSLA-100 steel to be a fine martensitic microstructure with a coarser granular bainite microstructure in the thicker plates (due to the slower cooling rates). Granular bainite consists of packets of ferrite laths with non-cementite, interlath, second phase particles of retained austenite or a combination of retained austenite and martensite. Examination of a 0.04%C HSLA-100 steel revealed a primarily bainitic microstructure as compared to the martensitic microstructure of the 0.06%C steel. The difference in microstructures illustrates the large impact of a small amount of carbon on an alloy's hardenability.

Wilson et al also investigated the copper precipitates found in HSLA-100 steel as part of their work. The copper precipitates were ϵ -copper and ranged in size from 2-25nm in diameter. The precipitates were found at dislocations within the ferrite grains, at ferrite lath boundaries and associated with bainite subboundaries.

The work of Czyryca and Link [Ref. 13: p. 16] confirmed the findings of Wilson et al and provided an explanation for the difference of Coldren and Cox's and Wilson et al's results. Czyryca and Link reported, as Wilson et al had, the microstructure of pro-

duction plates consisted of a mixture of low-carbon martensite and lower bainite in the thinner gages and of primarily bainite in the heavier gages. The discrepancy in the microstructures was attributed to the higher hot-rolling reductions and quenching rates available to the production plates as opposed to those used in the forming of the laboratory plates. The production plates also showed signs of manganese banding and were notably free of significant inclusions.

Howell [Ref. 22: p. 3-7] examined 31.75mm thick plates of the HSLA-100 trial production heat which had been solution treated at 899°C, water quenched, tempered at 565°C for 70 minutes and then air cooled to room temperature. He reported the microstructure had regions of aligned laths as well as regions with a more equiaxed appearance. The aligned laths were formed as ill-defined packets with the laths themselves on the order of 0.5 μ m wide. The lath structure was delineated by the presence of short segments of an aligned discontinuous phase. The remaining region had a granular morphology that arose from the presence of dispersed second phase particles within the irregularly formed grains of the matrix phase. Howell labelled the granular portion of the microstructure as found in the as-quenched state as granular bainite but called it granular ferrite when in the aged material. His reasoning for this labelling is as follows [Ref. 22: p. 4-5]:

The aligned lath ferrite microstructure in the as-quenched condition may be described variously as acicular ferrite, upper bainite, or lath martensite depending on the temperature range of formation. Fast quenching of low carbon HSLA steels from the solution treatment temperature leads to a predominantly lath martensitic microstructure whereas moderate quenching of very low carbon steels, e.g., HSLA-100 can result in a mixed bainite/lath martensitic microstructure. The bainite so formed may adopt either an aligned or what has been termed a granular morphology... On this basis, it is perhaps appropriate to refer to the irregularly formed ferrite microstructure with dispersed second phases in the quenched material as granular bainite... The granular bainite component upon aging may undergo some recovery resulting in a nearly equiaxed ferritic morphology with discrete metastable austenitic particles. Thus, the microstructure of the aged material would be predominantly tempered martensite/granular bainite. In the absence of any carbide... which is commonly associated with bainite and tempered martensite, the tempered materials could be characterized as granular ferrite.

Howell identified two lath structure types: long parallel laths such as those found in lath martensite and short laths such as those characteristic of acicular ferritic microstructures. The elongated laths, a few microns long and on the order of a few tenths of a micron in width, were heavily dislocated with the interlath boundaries clearly revealed on the most part by the presence of retained austenite. In addition to being found at

interlath boundaries, the retained austenite was also found within ferrite grains and at grain boundaries. The equiaxed grains were of the order of a few microns in diameter. The equiaxed and lath structure grain boundaries were mixed in their definition, some well defined and others blending together, implying the laths and granular ferrite had a common origin. [Ref. 22: p. 3-6]

Howell also investigated the precipitation of copper in HSLA-100 steel. His TEM examination revealed ε -copper dispersed throughout the entire ferritic microstructure. The dispersed ε -copper precipitates were similar in size to those found by Wilson et al, 2-30nm. Howell's research showed the ε -copper precipitation appeared to occur by heterogeneous nucleation on dislocations and at grain boundaries in ferrite and by interphase precipitation at the austenite/ferrite interface. Subsequent growth kinetics were controlled by the short circuit diffusion of the copper atoms along grain boundaries, dislocations and two-phase interfaces. The matrix precipitated ε -copper, most likely from supersaturated ferrite, was very uniformly distributed, very fine spherical particles while those which precipitated at grain boundaries were larger and had an elongated, rod-like appearance. The coarsest ε -copper particles were those which precipitated on austenite/ferrite interfaces. Since interface precipitation is a high temperature phenomena, this implied that the precipitates formed prior to or during the early stages of the quench from the solution treatment temperature. [Ref. 22: p. 6-7]

G. LOW-CARBON BAINITE STRENGTH AND TOUGHNESS PROPERTIES

The previous sections of this chapter have tried to explain the motivation for and the derivation of the microstructure of HSLA-100 steel as well as presenting the observations of several researchers investigating the microstructure of HSLA-100 steel. The object of this section is to establish the link between the bainitic microstructure of HSLA-100 steel and observed mechanical properties of HSLA-100 steel which are discussed in the next section.

As described by the research in the previous section, there are many definitions of just what bainite is, so a description of the microstructure of bainite will be the starting point for this discussion. Bainite is a microstructure that is the result of a low temperature transformation and consists of carbides dispersed in a ferrite matrix. In low carbon steel, bainite forms by a diffusion-controlled shear transformation of the prior austenite with the ferrite nucleating first. Two variants of bainite are possible, upper and lower bainite, both distinguishable by their morphology and the orientation relationship between the Fe_3C carbide and the ferrite matrix. [Ref. 9: p. 110]

1. Upper Bainite

In upper bainite, the shear transformation of the austenite results in plates or laths of ferrite which nucleate side by side in packets. At the higher temperatures at which upper bainite forms, the carbon is sufficiently mobile to diffuse in the austenite in front of the growing bainitic ferrite interface. The result is carbon-enriched austenite trapped between the bainitic ferrite laths. This carbon-enriched austenite can subsequently be retained as austenite, form high-carbon martensite or form Fe_3C between the ferrite laths, depending on the composition, degree of carbon enrichment, rate of cooling or the transformation temperature. The general structure consists of carbide films or elongated particles lying between the bainitic ferrite laths. If these carbides are retained austenite or martensite, the structure is termed granular bainite. The lower the transformation temperature, the finer the bainitic ferrite laths and the smaller and more numerous the carbides at the lath boundaries. [Ref. 9: p. 110-111]

2. Lower Bainite

Lower bainite forms at a lower transformation temperature than upper bainite, resulting in the nucleation of ferrite laths that are supersaturated with carbon since the carbon cannot diffuse away from the advancing bainite/austenite interface as readily as it can in upper bainite. To maintain the driving force for the transformation reaction, the carbon precipitates as small plates within the bainitic ferrite laths. Unlike upper bainite, the laths do not form side by side packets. The lower the transformation temperature, the finer the bainitic ferrite laths and the finer and more numerous the carbide particles. [Ref. 9: p. 111]

3. Strengthening Mechanisms

The following mechanisms are key components of the strength of bainitic steels [Ref. 9: p. 112]:

1. Fine bainitic lath size which gives a Hall-Petch relationship to strengthening:

$$\sigma_{ys} = \sigma_o + kd^{1-\frac{1}{2}}$$

The length of the lath depends on the prior austenite grain size while the lath width and the overall bainitic ferrite grain size decreases with decreasing transformation temperature.

2. The dislocation density which increases with a decrease in transformation temperature. The dislocations are due to the transformation strain but is increased further with increasing number of carbides.
3. The carbide dispersion which is increasingly effective with increasing carbon content and decreasing transformation temperature.

4. The carbon dissolved in the bainitic ferrite which increases with decreasing transformation temperature and causes solid solution strengthening and strengthening through interactions with dislocations.

The various modes of strengthening a bainitic steel have been combined in an empirical equation [Ref. 9: p. 113]:

$$0.2\% P.S.(MPa) = 15.4 \left[-12.6 + 1.13d^{\left(\frac{-1}{2}\right)} + 0.98n^{\left(\frac{1}{4}\right)} \right] \quad (2)$$

where d is the bainitic lath size (mean intercept length) in millimeters and n is the carbide distribution per square millimeter. The effect of the individual components of equation (2) can be seen in Figure 4 [from Ref. 9: fig. 6.11]. The negative constant indicates that there exists a threshold distribution of carbides below which the carbides do not contribute to the strength. This implies that the equation only applies to steels with finely distributed carbides, i.e. where the carbide spacing is less than the bainitic ferrite lath size. Therefore, in low carbon upper bainite, the strengthening is almost completely controlled by the bainitic ferrite grain size with the dislocation strengthening effect incorporated within the grain size effect since the dislocations generally form at the bainitic ferrite lath boundaries. In lower bainite, there is a significant contribution from the carbide dispersion as well as the grain size effect to the strength of the steel. The dislocation strengthening effect, rather than being a part of the grain size effect as in upper bainite, tends to be incorporated with the carbide dispersion effect. [Ref. 9: p. 1:3-4]

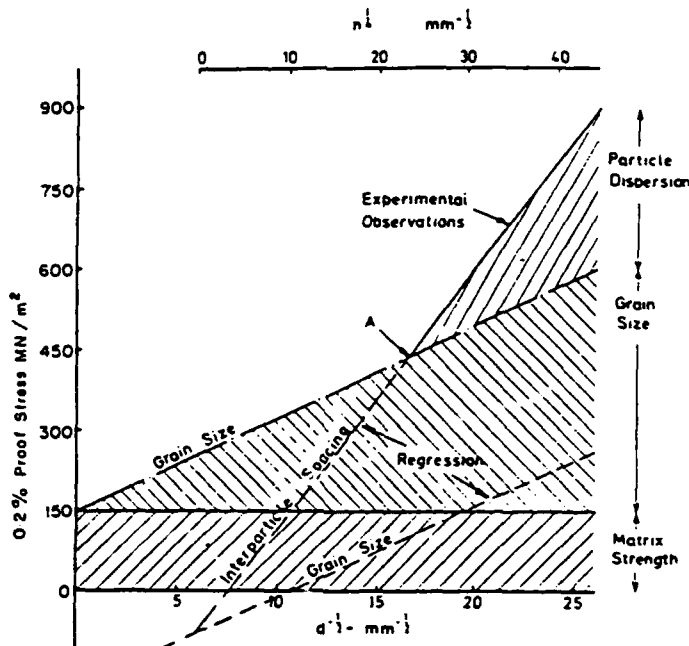


Figure 4. High Strength Bainite Strength Components

4. Toughness Properties

In upper bainite, the large carbides and high carbon martensite regions form a supercritical defect when cracked. Once initiated, the crack is not obstructed by the low angle bainitic ferrite lath boundaries but only by the high angle bainitic packet boundaries or prior austenite grain boundaries. Thus the crack tends to propagate rapidly. The impact resistance of the upper bainite can be improved primarily by refining the prior austenite grain size. Tempering will not aid the impact toughness behavior of upper bainite since no appreciable softening occurs until high tempering temperatures are used. Unfortunately, at the high tempering temperatures, the softening effect is countered by the growth of the ferrite grains. [Ref. 9: p. 116-7]

In lower bainite steels, the smaller carbides do not crack or, if they do, the defect is of subcritical size and there is no easy brittle failure. Once a crack is initiated, its propagation is obstructed by the many carbides and the increased dislocation density associated with lower bainite steel. The crack is frequently arrested and must continuously expend energy to reinitiate. When lower bainite is tempered, the reduction in strength is accompanied by a reduction of the impact toughness transition temperature as the beneficial distribution of carbides is retained (Figure 5 from Ref. 9: fig. 6.14). The tempering of lower bainite has the same problem as upper bainite at high temper-

atures as the ferrite grain growth results in an increase in the transition temperature (Figure 6 from Ref. 9: fig. 6.15). [Ref. 9: p. 117-118]

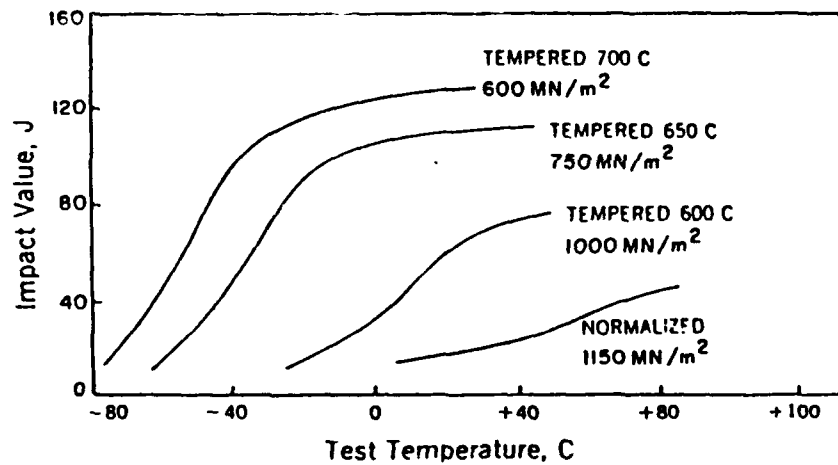


Figure 5. Bainitic Steel Tempering and DBTT

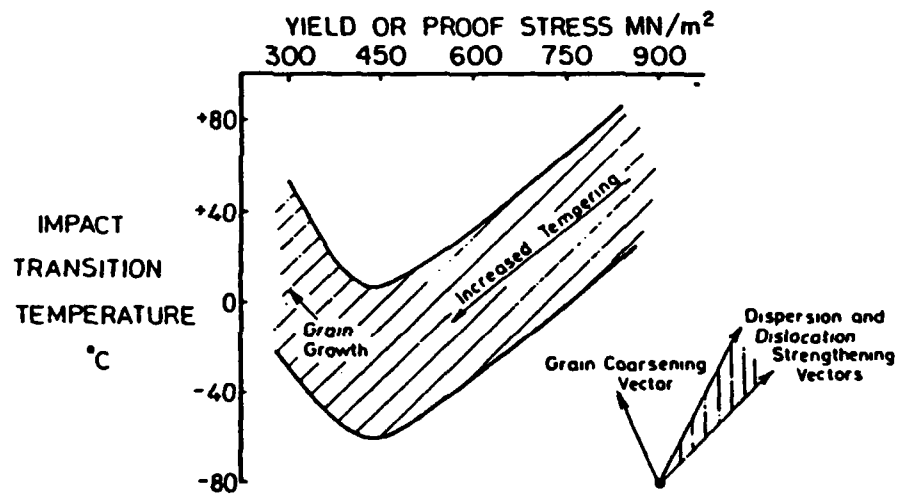


Figure 6. Tempered Bainite Steel Yield Stress and DBTT

H. MECHANICAL PROPERTIES OF HSLA-100 STEEL

HSLA-100 steel was designed to achieve a bainitic microstructure in order to take advantage of the excellent combination of toughness and strength properties normally associated with bainite while satisfying the requirements of Table 4. All HSLA-100 steel plates met the required minimum yield strength but the thinner plates required an aging at 690°C, which exceeds the 677°C lower transformation temperature (A_{C1}) and approaches the ferrite/austenite equilibrium temperature of 722°C, in order to remain below the required maximum yield strength [Ref. 2: p. 6]. Figure 7 (from Ref. 10: fig. 9, Ref. 23: fig. 11) shows the effect of aging on the yield strength. It is obvious from Figure 7 that the yield strength follows a classic copper precipitation strengthening profile with the peak strength occurring at 454°C.

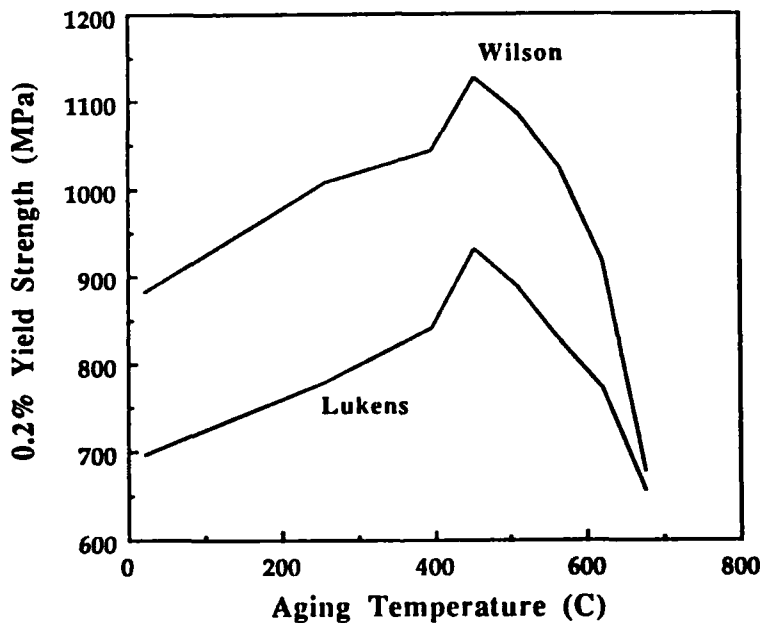


Figure 7. HSLA-100 Steel Yield Strength versus Aging Temperature

The toughness of HSLA-100 steel was measured by use of Charpy V-notch (CVN) impact tests on longitudinal (L-T) and transverse (T-L) orientation samples of each plate [Ref. 2: p. 7]. The results of the CVN tests were used to produce transition temperature plots for all the plates (Figure 9). All the HSLA-100 steel plates easily exceeded the requirements of Table 4, exhibiting upper shelf impact performance (100% shear fracture) to -51°C and a 50% fracture area transition temperature (FATT) below -84°C [Ref. 2 : p. 7]. When the CVN impact energy is plotted versus aging temperature (Figure 8),

some points of interest become apparent. The minimum in energy absorbed at -84°C and the maximum in FATT occur at peak strength as would be expected in a copper precipitation strengthened steel. A second and more interesting observation of Figure 8 is the toughness behavior at high aging temperatures where the toughness exceeds the as-quenched toughness by factors of up to 2. Wilson and Hamburg [Ref. 10: p. 265, Ref. 24] attribute this increased toughness to the nickel content, the more overaged condition of the copper precipitates and possibly the presence of tempered martensite.

Several other tests were conducted to get a measure of the toughness of HSLA-100 steel. Dynamic tear tests exceeded the minimum 678 J energy at -40°C required for HY-100 steel [Ref. 2: p. 7]. Elastic-plastic fracture toughness was measured throughout the ductile-brittle transition region using the J-integral method. In general, the fracture toughness of HSLA-100 steel exceeded that of HY-100 steel by factors of 2 to 2.5 [Ref. 2: p. 7]. The nil ductility temperature was determined, using the ASTM E208 drop-weight test method, to be -134°C [Ref. 2: p. 7].

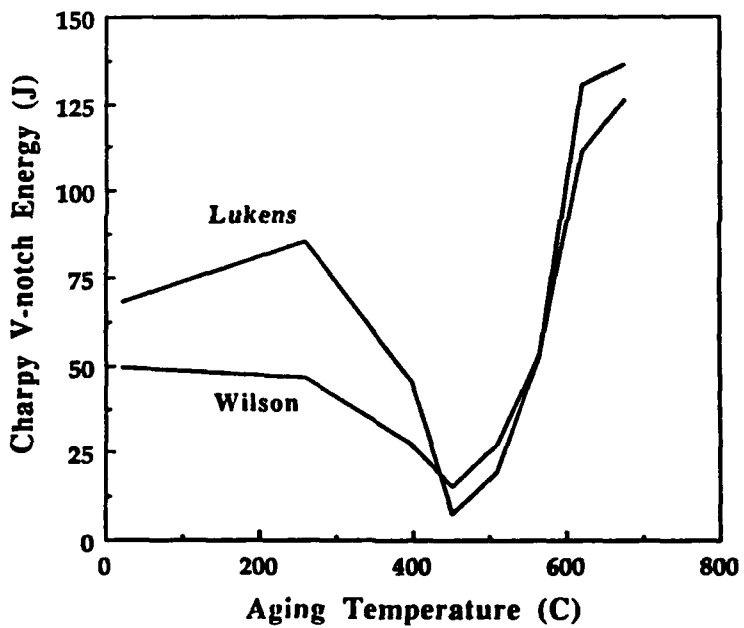


Figure 8. HSLA-100 Steel Charpy V-notch Energy versus Aging Temperature

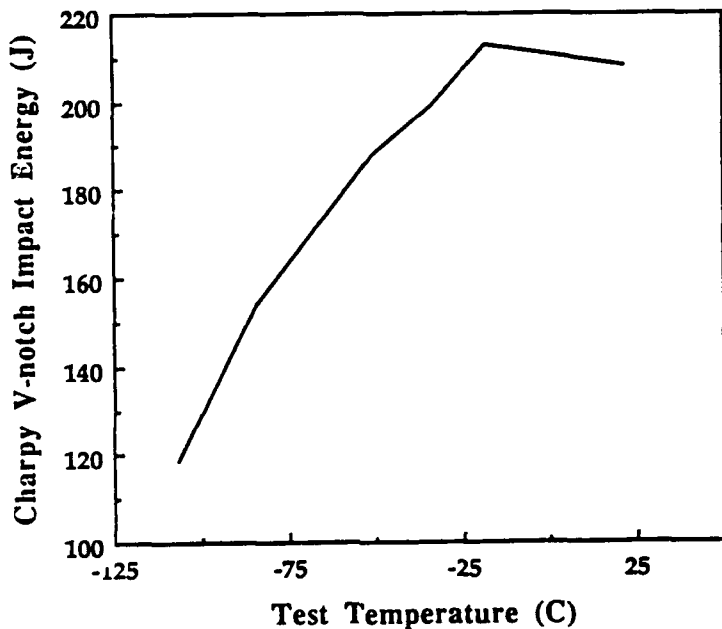


Figure 9. HSLA-100 Steel Charpy V-notch Energy Transition (1 in. thick)

Ductility of HSLA-100 steel was determined by measurement of elongation and reduction of area. Both criteria exceeded the requirements of Table 4 with elongations of 18 to 33% and reduction of area from 57 to 78%. [Ref. 2: p. 7]

Table 4. HSLA-100 STEEL STRENGTH AND TOUGHNESS REQUIREMENTS

0.2% Yield Strength	690 MPa minimum to 827 MPa maximum
Elongation	18% minimum in 50.8mm
Reduction of area	45% minimum
Transverse Charpy V-Notch Impact Toughness	81.3 J at -18°C; 54.2 J at -84°C

The elastic constants were measured in the transverse orientation to the plate's final rolling direction. The results were a modulus of elasticity (E) of 197 MPa and a Poisson's ratio (v) of 0.2916. The shear modulus, measured in torsion, averaged 80.7 MPa. [Ref. 2: p. 5]

I. SCOPE OF PRESENT WORK

The work on HSLA-100 steel to date has been concerned with the verification of mechanical and welding properties and the examination of the microstructure of the various gages and aging temperatures. General concensus is that HSLA-100 steel has a granular bainite microstructure with the interlath particles consisting of martensite and retained austenite in the as-quenched condition. Upon aging, copper precipitates to further strengthen the matrix. According to Wilson and Hamburg [Ref. 10 : p. 265 and Ref. 24], it is this overaged copper and the tempered martensite that provide the excellent toughness that HSLA-100 steel exhibits. The strength finds its basis in the fine grain size of the bainitic microstructure resulting from the refined prior austenite microstructure. Little work has been done on the possible contribution of the precipitation of niobium or molybdenum carbides to the strength or toughness of HSLA-100 steel. The object of this thesis is to examine the microstructural basis for the strength and toughness properties of HSLA-100 steel, in particular the overaged steels where anomalously high fracture toughnesses have been observed.

III. EXPERIMENTAL PROCEDURE

A. MATERIAL

Seven HSLA-100 plate steel Charpy sample halves were provided by the David Taylor Research Center (DTRC), Annapolis, Maryland. The samples were from the same Lukens Steels Co., Coatesville Works lot (DTRC code GQH). The melts were formed in electric arc furnaces, Al-killed and argon-injected with CaSi and then vacuum degassed. Ingots were bottom poured and hot charged. The ingots were then reheated to approximately 1177°C, cut into smaller slabs and rolled to a finishing temperature of 954°C and a thickness of 31.75mm [Ref. 25]. The Charpy samples were cut from the plate along the T-L orientation. The samples were austenitized for one hour at 899°C, then quenched and aged at temperatures of 399, 454, 510, 566, 621, and 677°C for 75 minutes by DTRC. One as-quenched sample was also provided. Table 5 provides the chemical composition of the lot as determined by DTRC.

Table 5. HSLA-100 STEEL LOT GQH CHEMICAL COMPOSITION

C	Mn	Ni	Cr	Mo	Cu
0.048	0.69	3.42	0.52	0.54	1.47
Nb	Si	P	S	N	O
0.020	0.27	0.010	0.004	0.0091	0.0035

B. MECHANICAL PROPERTIES

Charpy V-notch impact energy, yield strength, tensile strength and ductility testing was conducted by DTRC and the data provided to the author. The dimensions of the bainite packets were measured using TEM micrographs and back-scattered electron SEM micrographs similar to Figure 10. The bainite packet size was measured using a mean intercept method on the SEM micrographs while the bainite lath lengths were averaged from those on the same SEM micrographs. The bainite lath widths were measured using a mean intercept method on the TEM micrographs due to their fine size.

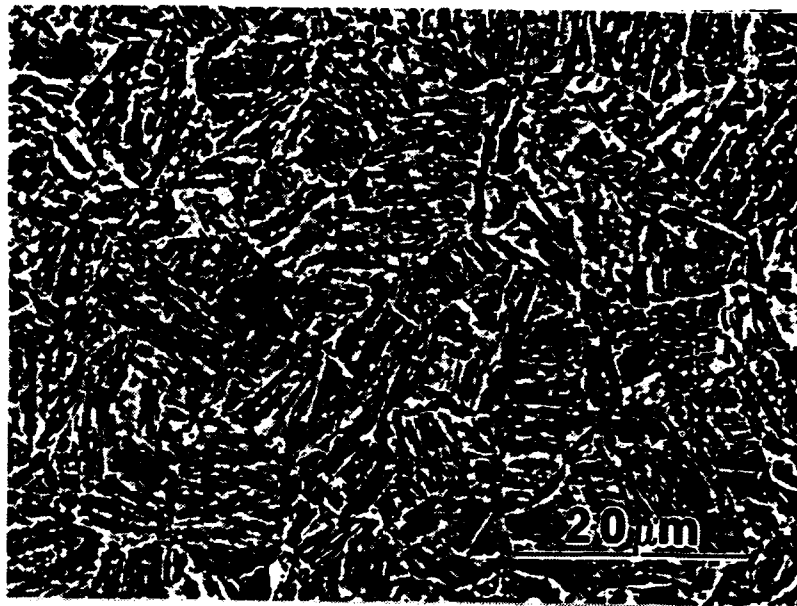


Figure 10. 566°C Aged HSLA-100 Steel Back-Scattered SEM Micrograph

C. MICROSCOPY

1. Optical Microscopy

A metallographic sample was prepared from the as-quenched and 454, 566 and 677°C Charpy samples and mounted, polished and etched for approximately 20 seconds using a two percent nital etching solution. Each sample was examined and photographed in a Zeiss ICM405 photomicroscope.

2. Scanning Electron Microscopy

Polished samples of the as-quenched and the 454, 566 and 677°C aging temperature Charpy samples were examined in a Cambridge Stereo Scan S200 Scanning Electron Microscope to investigate the inclusion content by type and size. Chemical analysis of the inclusions was conducted with a Kevex 8000 EDX Spectrometer. Photographs of etched samples were taken for use in determining bainite packet size and lath length.

3. Transmission Electron Microscopy

Discs were cut from the as-quenched and the 454, 566 and the 677°C aging temperature Charpy samples using a low-speed diamond wafering saw and mechanically thinned on wet 600 grit silicon carbide paper to a thickness of less than 0.05mm. The discs were electrochemically thinned to perforation in a Struers Tenupol electropolishing

device, operated at 70 volts and a medium flow rate, using a 3% perchloric acid, 35% n-butoxy ethanol and 62% ethanol solution, cooled to -35°C with liquid nitrogen. After thinning, the discs were ion milled in a Gatan Dual Ion Mill (Model 600) at room temperature using two guns at gun currents of 0.5 to 1.0 milliamperes (DC) for two minutes in order to remove copper that redeposits on the discs during the electropolishing process. The discs were examined and photographed on a JEOL model JEM 100CX transmission electron microscope operated at 120KV. Micrographs taken of the samples were used in determining bainite lath width and examining other microstructural features such as retained austenite, carbides and copper precipitates. The as-quenched and 677°C aged discs were also examined and X-ray mapped with a JEOL model JEM 200CX scanning transmission electron microscope operated at 200KV at the National Center for Electron Microscopy located at the Lawrence Berkeley Laboratory, Berkeley, California.

IV. EXPERIMENTAL RESULTS

A. MECHANICAL BEHAVIOR

The variation of yield strength and ultimate tensile strength with aging temperature are presented in Figure 11 and Figure 12. Both the yield strength and the ultimate tensile strength reach a maximum at 454°C and then decrease at higher aging temperatures. The decrease in strength increases markedly above 677°C. The strength behavior very closely resembles that of previously published data, Figure 7, and exhibits the characteristic aging behavior associated with copper precipitation.

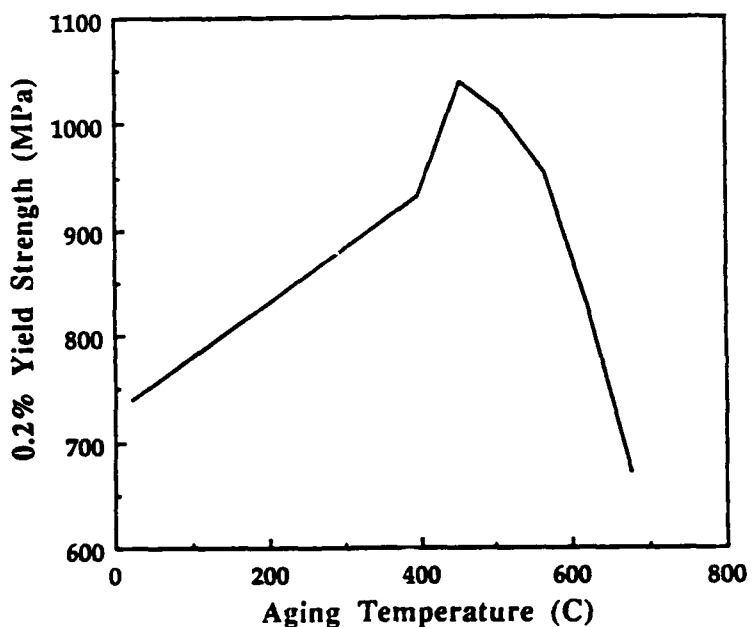


Figure 11. HSLA-100 Steel Lot GQH 0.2% Yield Strength

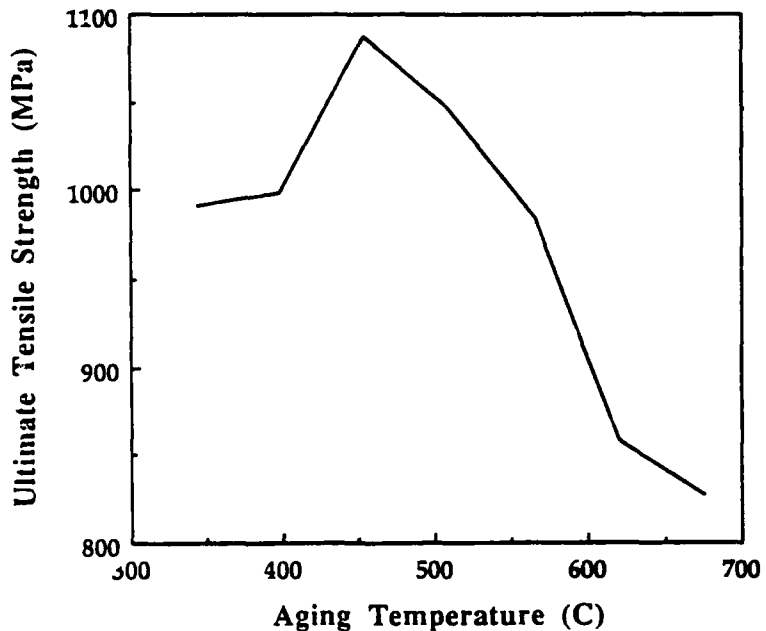


Figure 12. HSLA-100 Steel Lot GQH Tensile Strength

The effect of aging temperature on the impact energy at -84°C is shown in Figure 13. The impact energy responds in a manner as would be expected for a copper age-hardened steel. The toughness decreases to a minimum as the aging temperature increases up to the peak age temperature (454°C). Above the 454°C aging temperature, the toughness increases with aging temperature. A significant increase occurs above the 566°C aging temperature where the impact energy exceeds the as-quenched steel by a factor of 2. This behavior of HSLA-100 steel can also be seen in the DBTT curves, Figure 14. As the aging temperature is increased to 566°C , the impact energy decreases to a minimum at the 454°C aging temperature and then returns to approximately the same impact behavior at 566°C as it had in the as-quenched condition. Aging above 566°C results in a marked increase in the impact energy at all testing temperatures and decrease in the DBTT. While traditional copper age-hardened steels do respond in a similar manner when aged, they do not experience the significant increase in toughness or decrease in yield strength seen in HSLA-100 steel at high aging temperatures. It would seem that although copper does play a major role in the toughness and strength behavior of HSLA-100 steel, other microstructural factors play an important role at high aging temperatures.

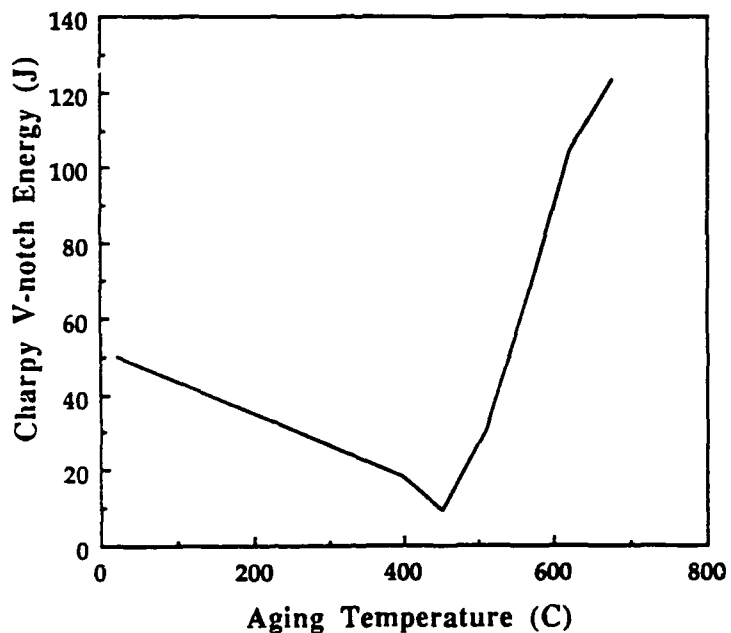


Figure 13. HSLA-100 Steel Lot GQH Impact Energy at -84°C : Variation of impact energy with aging temperature.

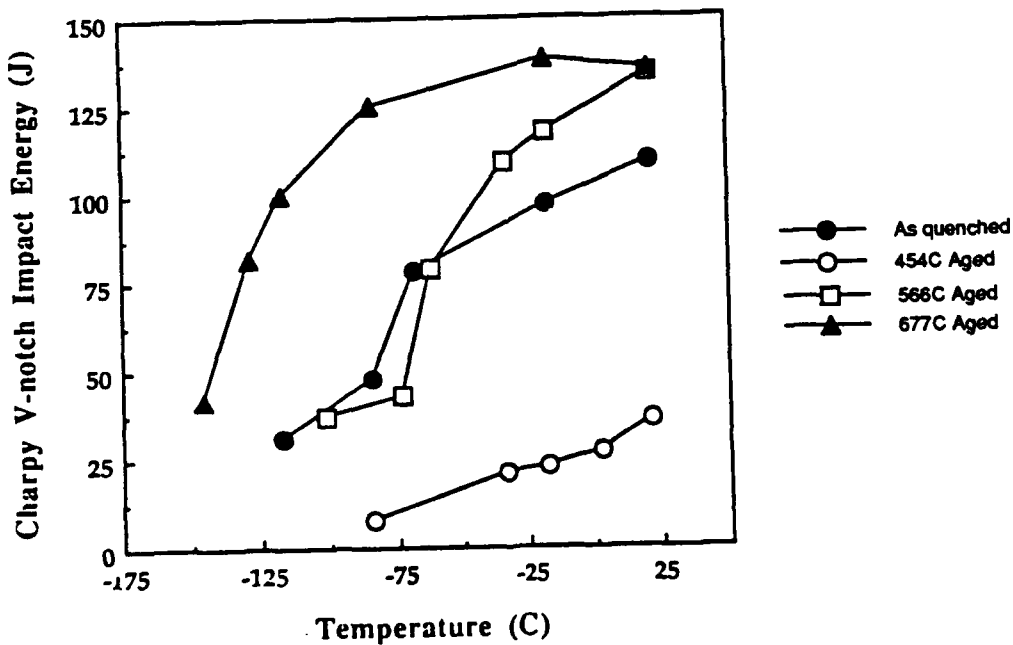


Figure 14. HSLA-100 Steel Lot GQH DBTT: DBTT behavior for various aging temperatures.

The ductility of HSLA-100 steel as a function of aging temperature is shown in Figure 15. The elongation increases gradually from 23% to 42% while the reduction of area remains essentially constant varying only 5%, from 68 to 73%. Both are relatively insensitive to the aging temperature, the reduction of area measurement more so than the elongation measurement. This is in direct contrast to the significant dependence of the impact toughness on the aging temperature. Since ductility is essentially a function of dislocation motion and toughness a function of dislocation motion and crack propagation and arrest, it is would seem the key to the toughness of HSLA-100 steel is crack propagation and arrest.

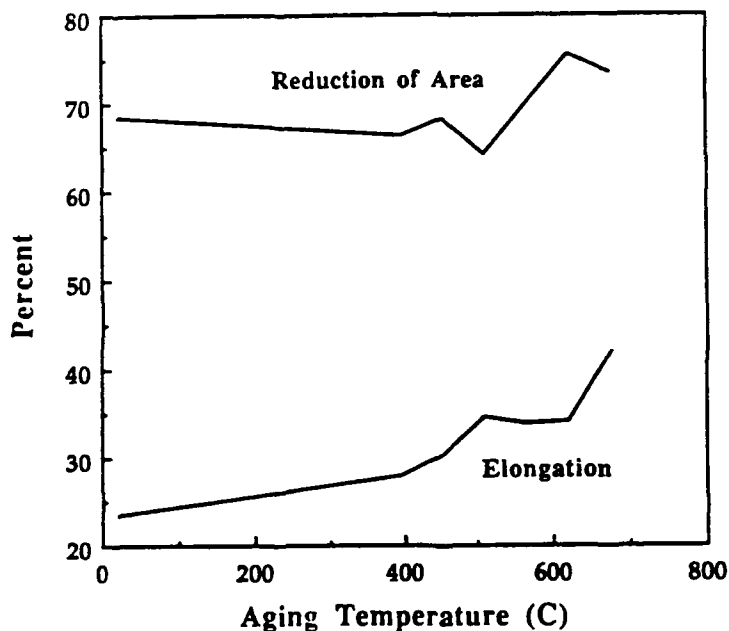


Figure 15. HSLA-100 Steel Lot GQH Ductility: Variation of elongation and reduction of area with aging temperature.

Figure 16 illustrates the growth of the bainite microstructure as a function of aging temperature. The bainite lath length and the bainite packet size under go very slow growth up to 566°C. Above 566°C, these two dimensions experience very rapid growth. The bainite lath width grows very slowly up to the peak age temperature, 454°C, and then under goes rapid growth at higher aging temperatures. The overall result is slow grain growth up to 454°C, followed by an widening of the laths to form more equiaxed

grains and finally by significant uniaxial grain growth above 566°C. Comparison of this bainite grain growth with the behavior of the mechanical properties indicates a significant microstructural change occurs at or near the 677°C aging temperature. This very closely resembles the conclusions of Heinze [Ref. 26] who also attributed observed significant changes in strength and ductility above 675°C to a microstructural change.

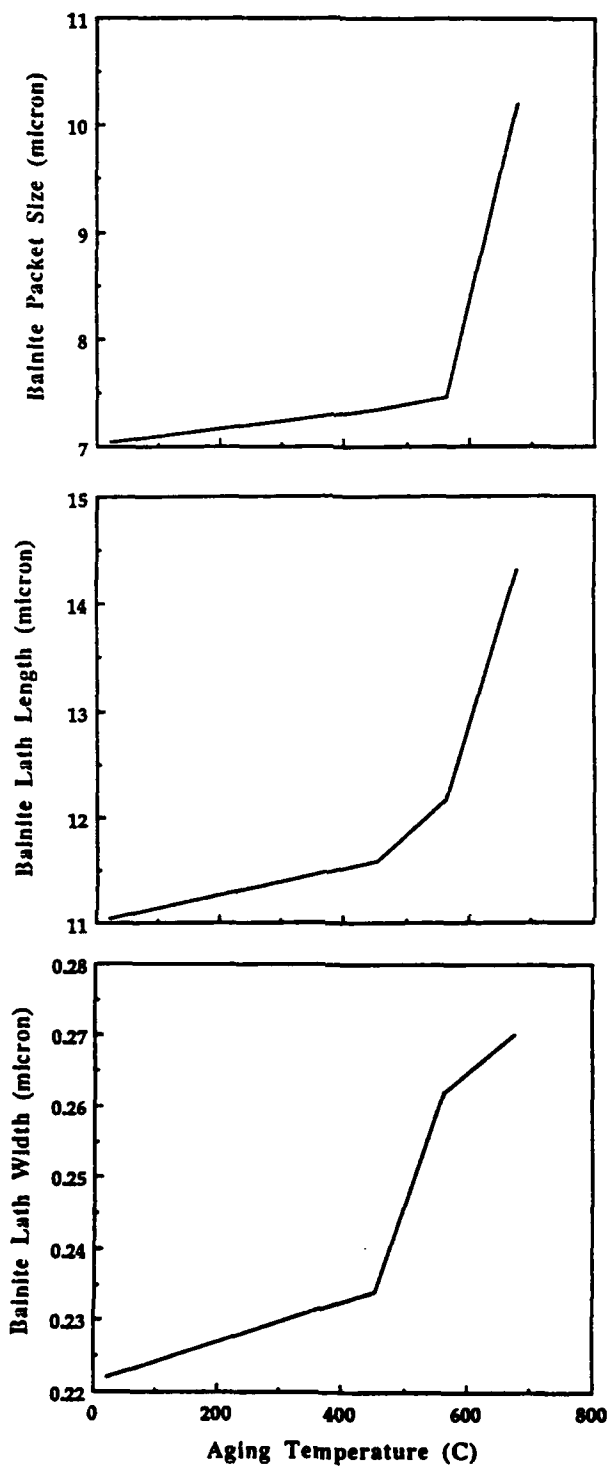


Figure 16. HSLA-100 Steel Lot GQH Bainite Parameters: Variation of bainite packet size, lath length and lath width with aging temperature.

B. MICROSTRUCTURE

1. As-quenched HSLA-100 Steel

Light and SEM micrographs of the as-quenched HSLA-100 steel are shown in Figure 18. The high-angle boundaries visible are prior austenite grain boundaries. The SEM micrograph shows the granular bainite grain structure in greater detail. The aligned lath ferrite (A) and the dispersed second phase particles (B) associated with granular bainite are visible. Normally in granular bainite the lath structures are separated by cementite but the low carbon content of HSLA-100 steel precludes the formation of cementite and the particles in (B) are retained austenite or martensite. Figure 17 is a TEM micrograph illustrating several bainite laths. The low-angle interface between the laths is visible as is the high dislocation density (A). The laths themselves are generally precipitate free. The as-quenched sample contains retained austenite, as seen in Figure 19, and martensite, seen in Figure 20. The high dislocation density associated with martensite is visible at (A) in Figure 20. Retained austenite can also be seen in the dark field micrograph, Figure 23. This dark field was obtained by illuminating spot A in the selected area diffraction pattern (SADP), Figure 21, of Figure 22. The SADP itself is clear of the streaking associated with the precipitation of coherent BCC copper zones and has relatively few extra spots, indicating most of the alloying elements that could precipitate, i.e. copper, niobium and molybdenum, have remained in solid solution. The extra diffraction spots are due to austenite and martensite within the microstructure and appear because the selected area the diffraction aperture covers is greater than the width of a single bainite lath.



Figure 17. TEM Image of As-quenched HSLA-100 Steel Lath Structure: \bar{B} close to $<110>$, $\bar{g} = 110$ type.

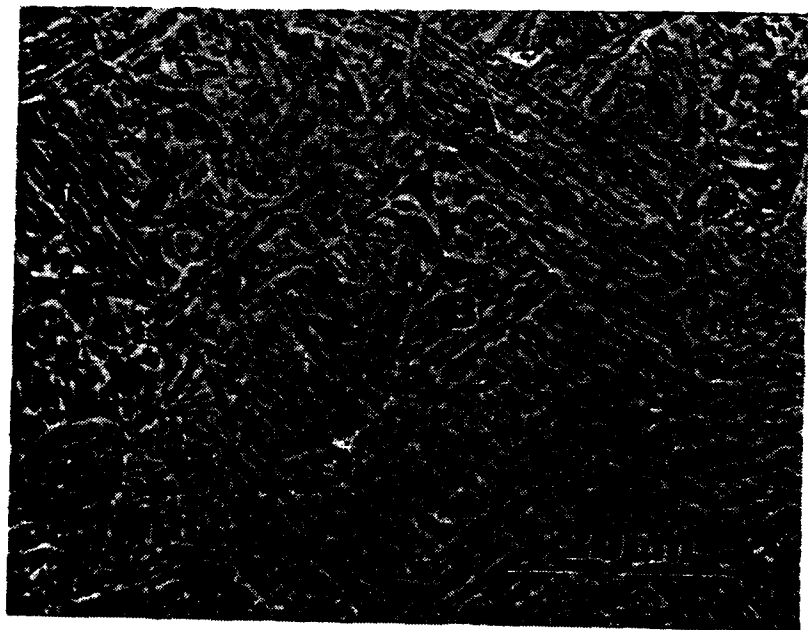


Figure 18. Micrographs of As-quenched HSLA-100 Steel Grain Structure: (Top) Light Micrograph, (Bottom) Secondary Electron SEM Micrograph.



Figure 19. TEM Images of As-quenched HSLA-100 Steel Retained Austenite: \bar{B} close to $\langle 133 \rangle$, $\bar{g} = 110$ type; (Top) Bright field, (Bottom) Dark field.



Figure 20. TEM Images of Martensite in As-quenched HSLA-100 Steel: \bar{B} close to $<133>$, $\bar{g} = 110$ type; (Top) Bright field, (Bottom) Dark field.

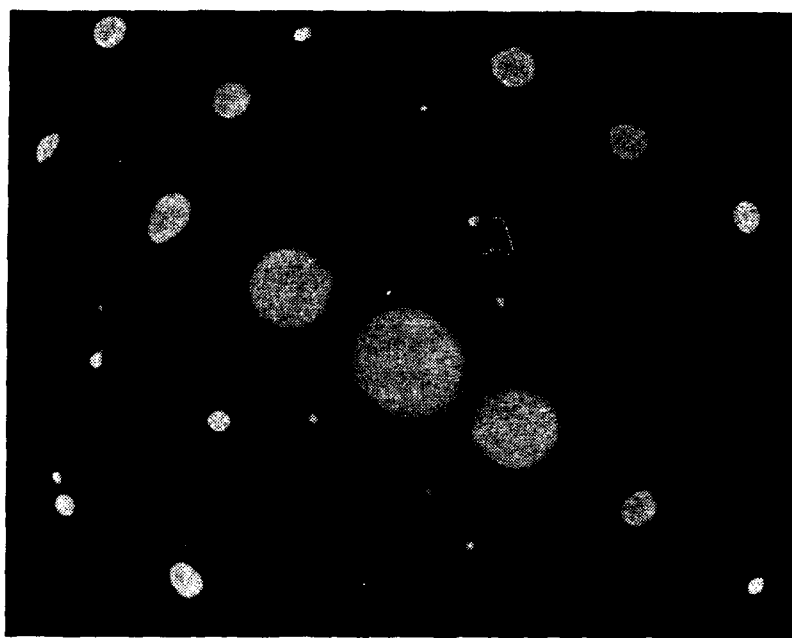


Figure 21. As-quenched HSLA-100 Steel SADP: \vec{B} close to $\langle 133 \rangle$, $\vec{g} = 110$ type.

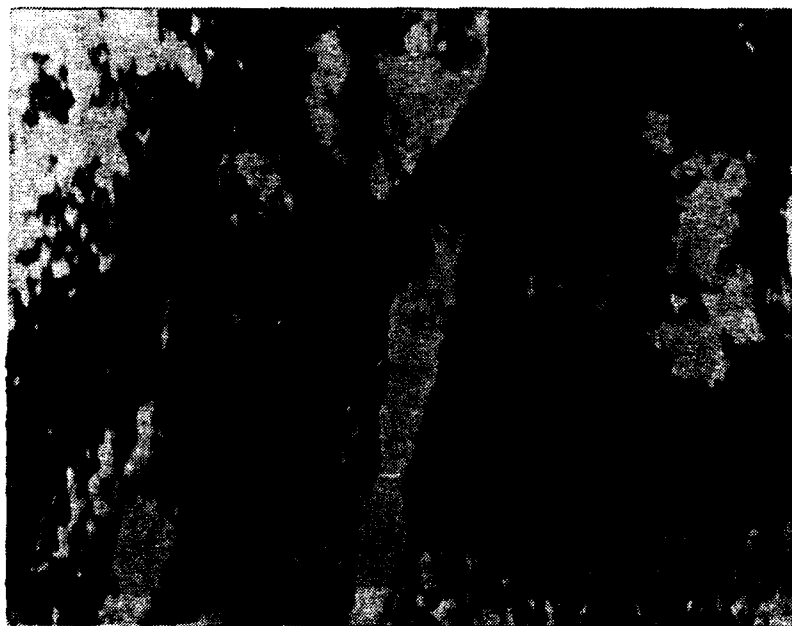


Figure 22. TEM Bright Field Image of Retained Austenite in As-quenched HSLA-100 Steel: \vec{B} close to $\langle 133 \rangle$, $\vec{g} = 110$ type.

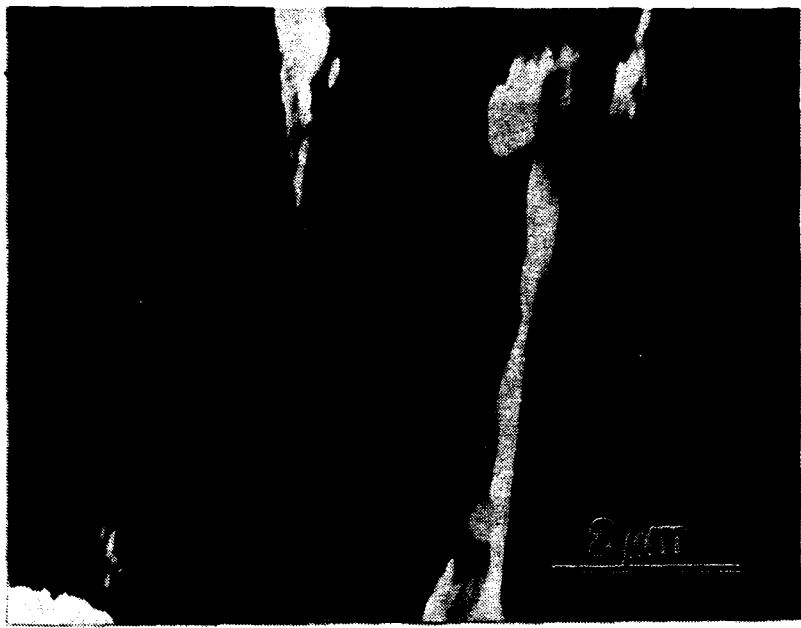


Figure 23. TEM Dark Field Image of Retained Austenite in As-quenched HSLA-100 Steel: \bar{B} close to $\langle 133 \rangle$, (ferrite).

2. 454°C Aged HSLA-100 Steel

The microstructure of the peak aged HSLA-100 steel is shown in Figure 24. The individual laths are not as easily distinguishable as they were in the as-quenched condition. The bainite packets are approximately the same size but are more equiaxed due to the growth in the width of the laths. The dispersed second phase, prominent in the as-quenched condition, is not as visible. The lath structure is shown in Figure 25. Regions of high dislocation density are visible (A) but they are not as extensive as in the as-quenched sample due to recovery that has occurred. The precipitated coherent BCC copper zones cannot be imaged due to their small size but their coherency strain fields are visible in Figure 26 and Figure 27. The coherent BCC copper zones effect on the SADP, Figure 28, is seen in the streaking. The precipitation of carbides is the source of the numerous regularly spaced spots in the SADP. Intralath carbides, on the order of 70-300Å in length, are shown in Figure 29, a dark field image of diffraction spot A on Figure 28. Interlath carbides (A) are seen in Figure 31. The interlath carbides vary

from 300 to 500Å in length and may be the result of the tempering of martensite. Regions of martensite remain as seen in Figure 30.



Figure 24. Micrographs of 454°C Aged HSLA-100 Steel Grain Structure: (Top) Light Micrograph (Bottom) Secondary Electron SEM Micrograph.

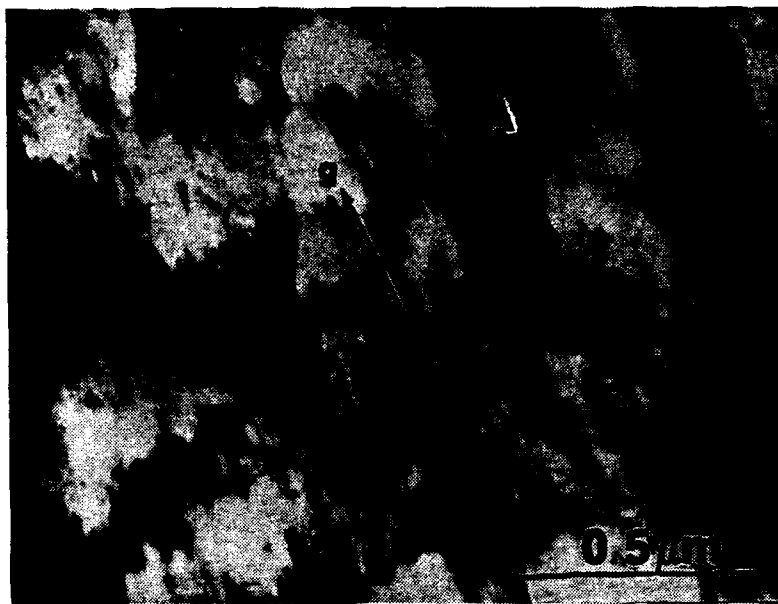


Figure 25. TEM Image of 454°C Aged HSLA-100 Steel Lath Structure: \vec{B} close to $\langle 113 \rangle$, $\vec{g} = 110$ type.

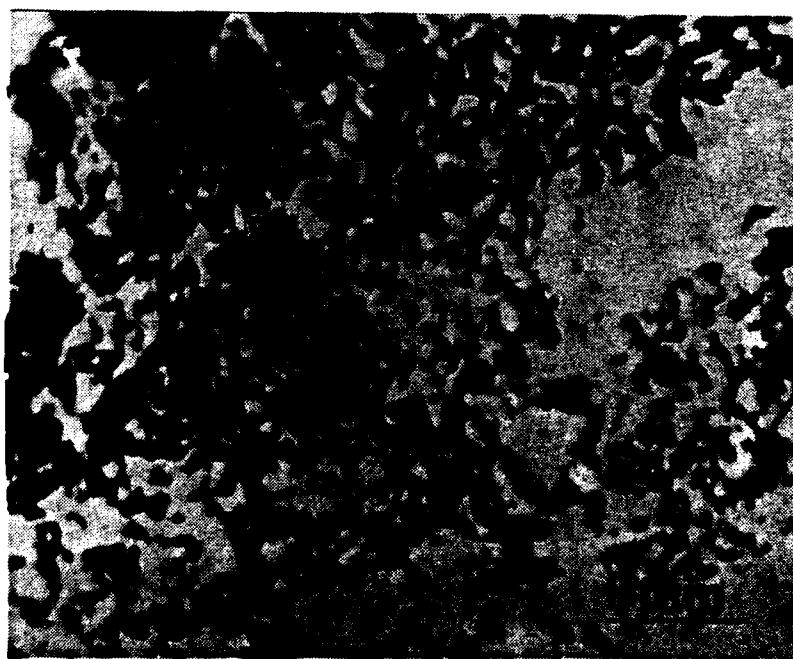


Figure 26. TEM Image of 454°C Aged HSLA-100 Steel Copper Coherency Strain Field: \vec{B} close to $\langle 110 \rangle$, $\vec{g} = 112$ type.



Figure 27. TEM Image of 454°C Aged HSLA-100 Steel Copper Coherency Strain
Field: \vec{B} close to $\langle 113 \rangle$, $\vec{g} = 110$ type.

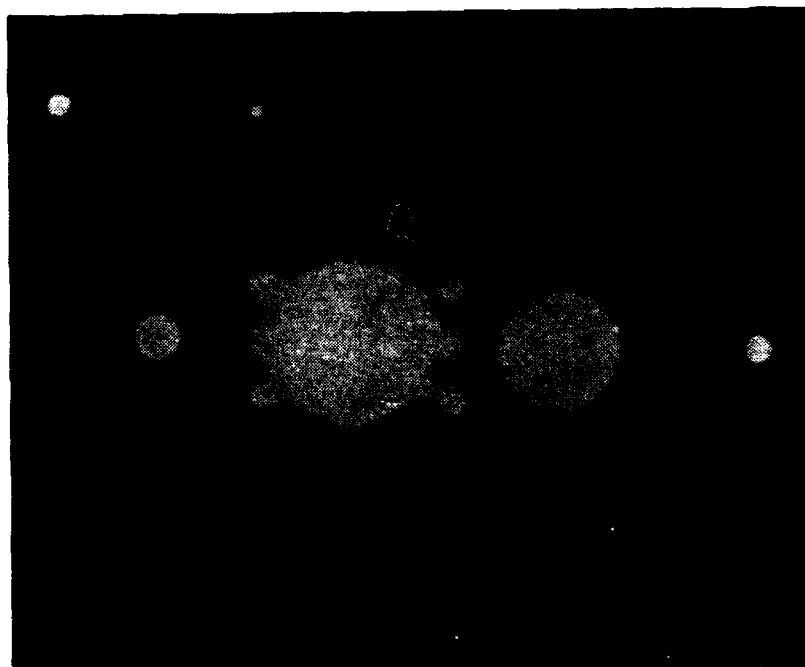


Figure 28. 454°C Aged HSLA-100 Steel SADP: \vec{B} close to $\langle 113 \rangle$, $\vec{g} = 110$ type.

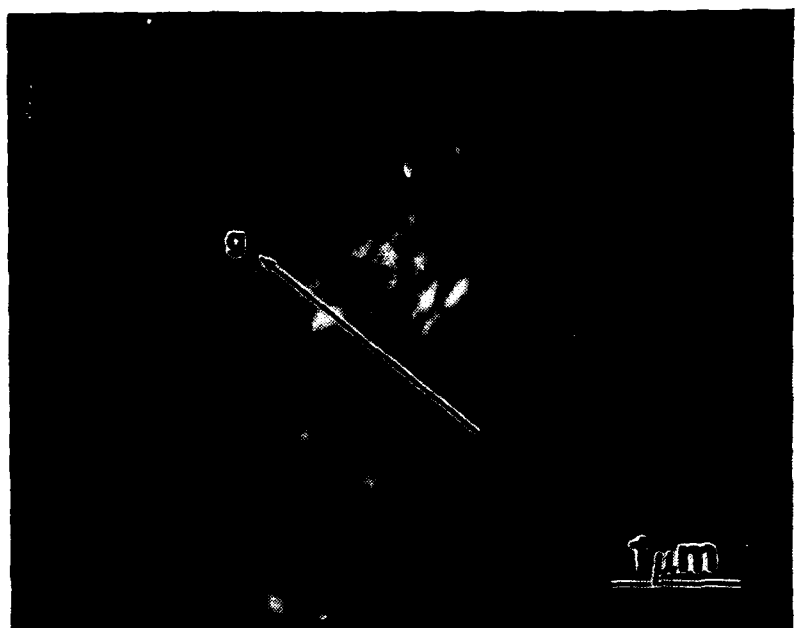


Figure 29. TEM Dark Field Image of 454°C Aged HSLA-100 Steel Intralath Carbides: \bar{B} close to $<113>$, (ferrite).

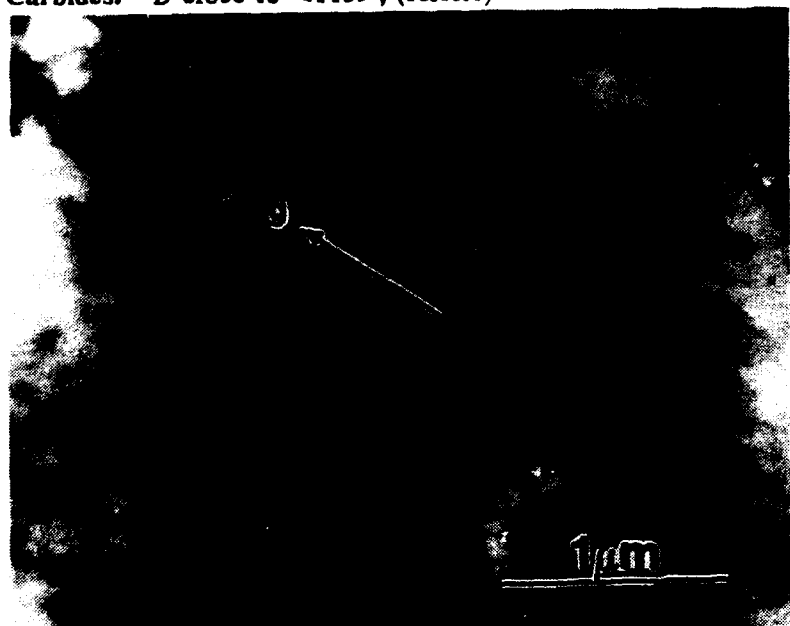


Figure 30. TEM Image of Martensite in 454°C Aged HSLA-100 Steel: \bar{B} close to $<012>$, $\bar{g} = 200$ type.

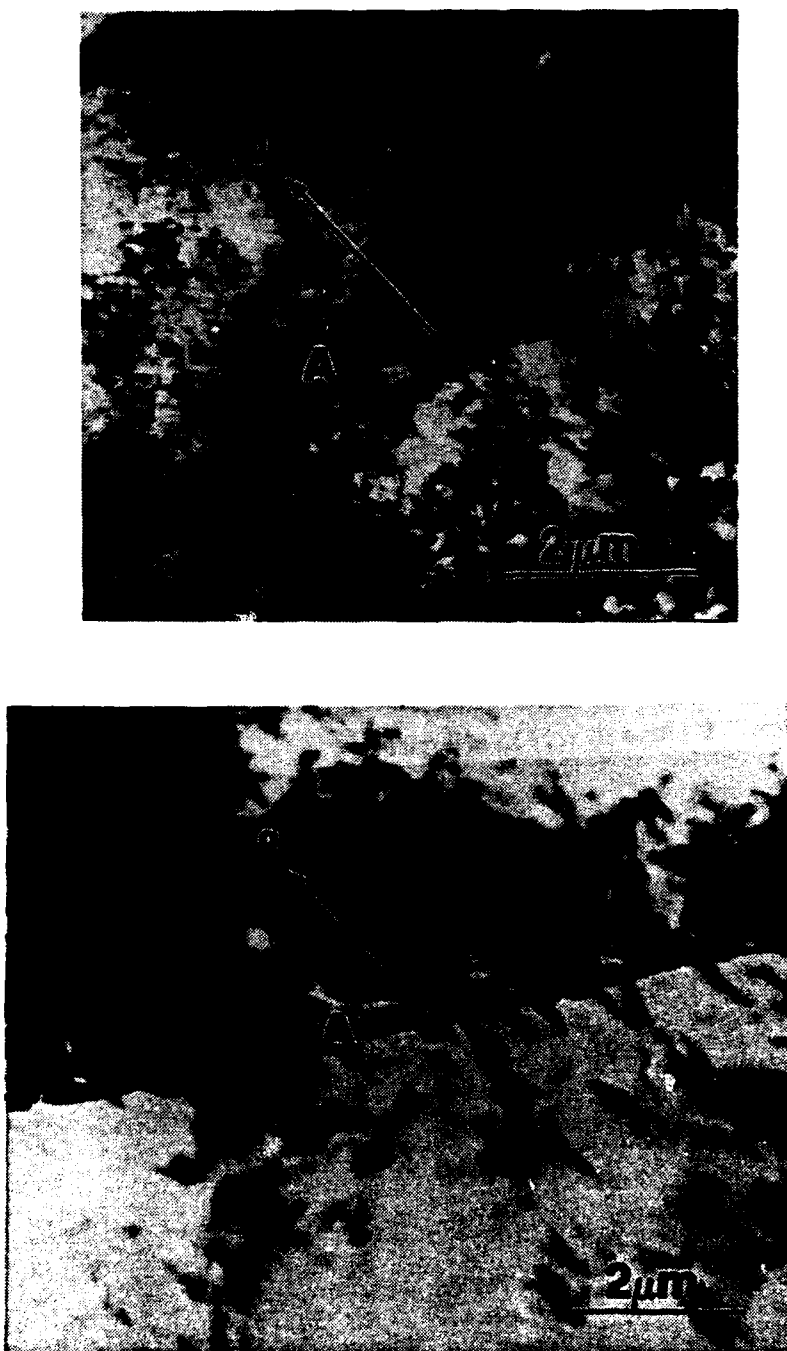


Figure 31. TEM Images of 454°C Aged HSLA-100 Steel Interlath Carbides: \bar{B} close to $\langle 012 \rangle$, $\bar{g} = 200$ type.

3. 566°C Aged HSLA-100 Steel

The light and SEM micrographs, Figure 32, do not reveal any significant microstructural differences when compared to the 454°C aging temperature. The TEM micrograph of the lath structure shows the regions of dislocations are of less intensity than the previous two samples and the laths have continued their widening. Interlath martensite is visible at A. The significance of this aging temperature is the loss of the streaking on the SADP, Figure 34, due the transformation of the copper precipitates from BCC to FCC. The uniformly distributed copper particles are visible as spherical 50Å precipitates in Figure 36. The size and shape of the copper precipitates correlates well with the 40Å copper particle diameter observed by Goodman, Brenner and Low [Ref. 18: p.2377].

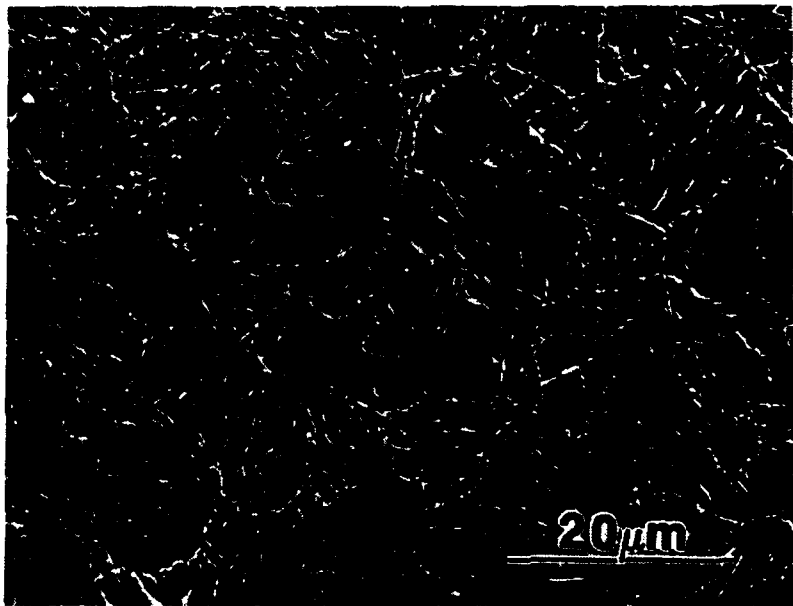
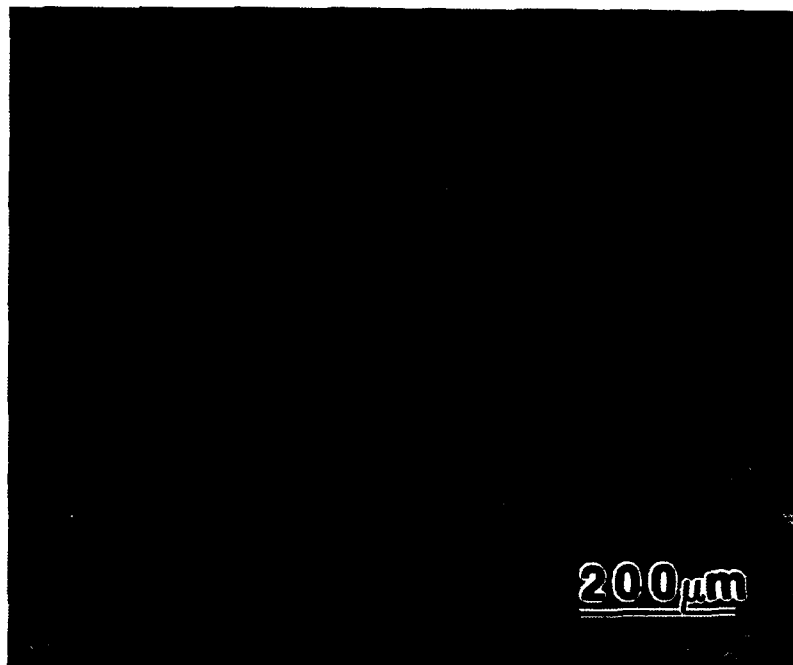


Figure 32. Micrographs of 566°C Aged HSLA-100 Steel Grain Structure: (Top) Light Micrograph, (Bottom) Secondary Electron SEM Micrograph.



Figure 33. TEM Image of 566°C Aged HSLA-100 Steel Lath Structure: \vec{B} close to $<012>$, $\vec{g} = 200$ type.

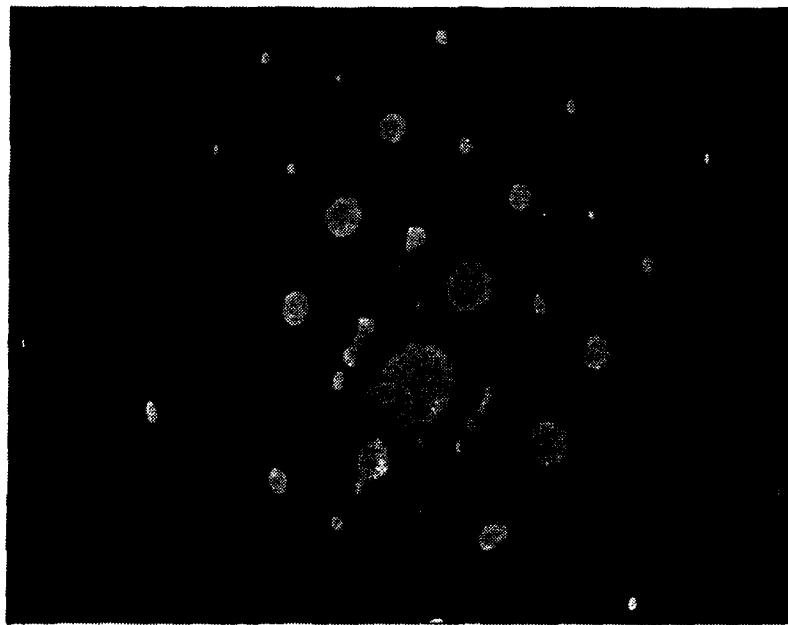


Figure 34. 566°C Aged HSLA-100 Steel SADP: \vec{B} close to $<110>$, $\vec{g} = 110$ type.

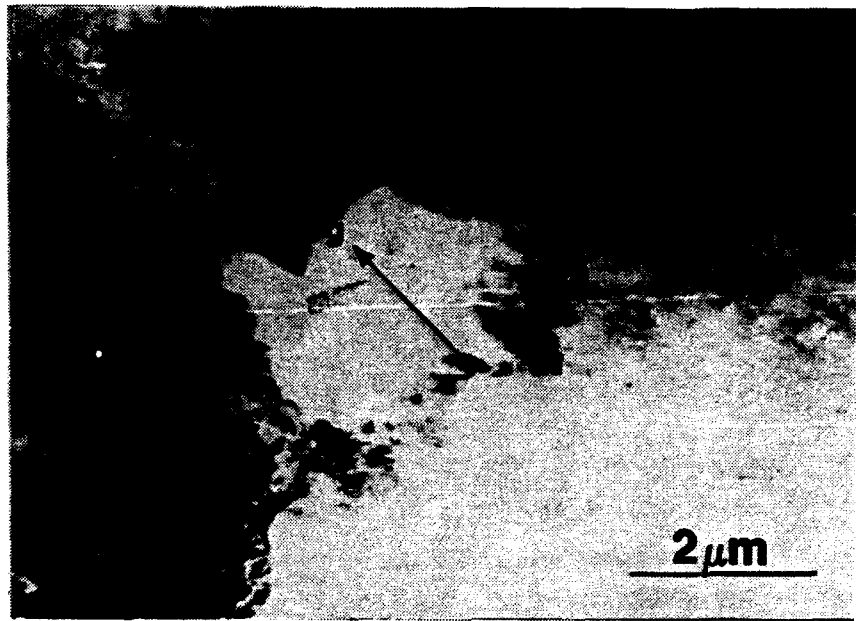


Figure 35. TEM Bright Field Image of Copper Precipitates in 454°C Aged HSLA-100 Steel: \bar{B} close to $\langle 110 \rangle$, $\bar{g} = 200$ type.

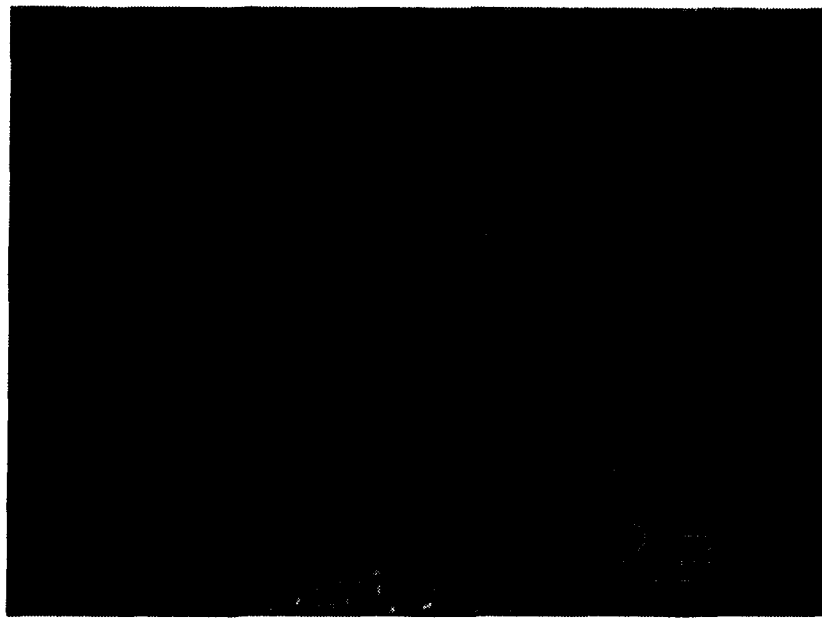


Figure 36. TEM Dark Field Image of Copper Precipitates in 454°C Aged HSLA-100 Steel: \bar{B} close to $\langle 110 \rangle$, (Copper FCC spot).

4. 677°C Aged HSLA-100 Steel

Figure 37 shows light and SEM micrographs of the 677°C aged HSLA-100 steel. Significant grain growth has occurred and regions which appear ferrite-like are forming (A), distinguished by the high contrast, high angle boundaries. The lath structure, while visible in the TEM, is less distinctive in the light and SEM micrographs. Study of the lath structure in the TEM shows that areas of ferrite have formed (A in Figure 38). The formation of ferrite is due to aging the steel at the lower transformation temperature, 677°C [Ref. 2: p. 6], which allows recrystallization to occur. Because little energy is available for the driving force of recrystallization, only high energy regions of high dislocation density recrystallized. This is what appears to have happened at B in the bottom micrograph of Figure 38. The bainite laths extending from the lower left of the micrograph abruptly end at various lengths, not the uniform length normally seen, giving way to a cluster of ferrite grains. The region of ferrite grains most likely was an area of high dislocation density. The result is the growth of fine, ferrite grains. The ferrite grains are distinguished by their high angle boundaries which cause a contrast distinction between neighboring grains. The dual-phase microstructure consists of low-angle boundary bainite laths, high-angle boundary ferrite grains and martensite. A high magnification micrograph of the lath structure, Figure 39, shows the minimal dislocation density, copper precipitates (C), and possible carbides. The complexity of this steel can be seen in the SADP, Figure 40, where the multitude of spots are the result of various forms of Nb- and Mo-carbides precipitating as well as copper precipitation and remaining martensite.

The micrographs in Figure 41 illustrate both inter- and intralath carbides. The interlath carbides are elongated 500-1000Å particles while the intralath particles are 50-100Å spherical precipitates. EDX spectra (Figure 42) shows the interlath carbides are molybdenum based. X-ray mapping shows molybdenum is prominent at lath or prior austenite grain boundaries (Figure 43). The intralath carbides were found to contain niobium as well as molybdenum (Figure 42).

The X-ray mapping also shows copper precipitation (Figure 43). While the distribution was generally uniform, larger concentrations of copper are seen at lath boundaries. Lath boundary precipitation is seen in Figure 44. Evidence of copper precipitation within the bainite laths is seen in Figure 46 and on dislocations in Figure 45. The overaged copper precipitates are oblong and vary from 300 to 1000Å in length.

Many of the copper particles are distinguished by stacking faults. The stacking faults are parallel to the long axis of the precipitates as should be expected since the preferred growth direction is $<110>$, which lies in the (111) plane [Ref. 15: p. 1068] and the {111} planes are the FCC close packed planes and have the lowest stacking fault energy [Ref. 27: p. 796-7].

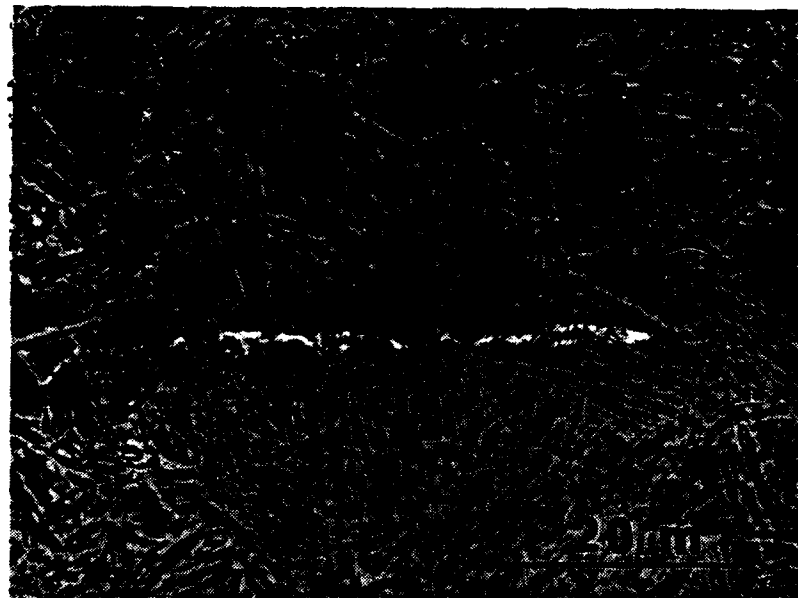
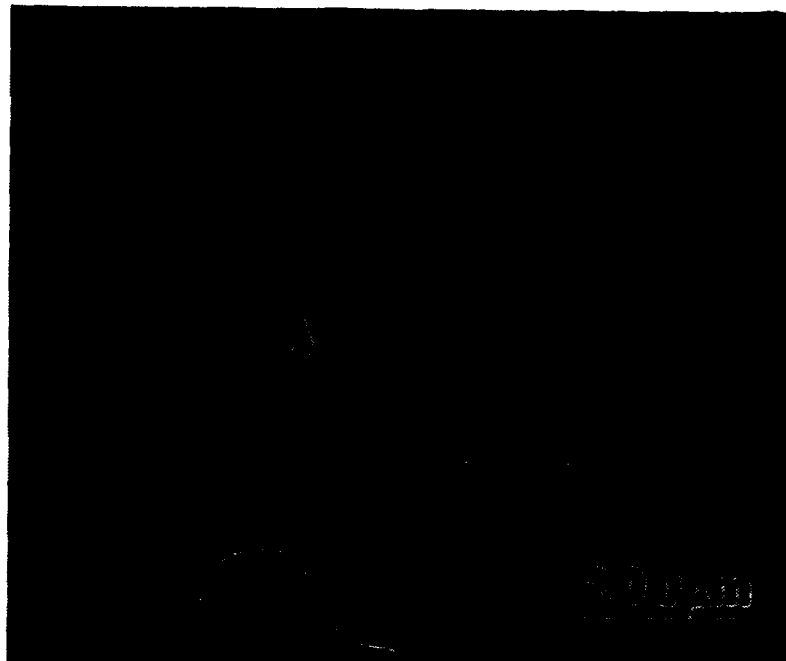


Figure 37. Micrographs of 677°C Aged HSLA-100 Steel Grain Structure: (Top) Light Micrograph, (Bottom) Secondary Electron SEM Micrograph.

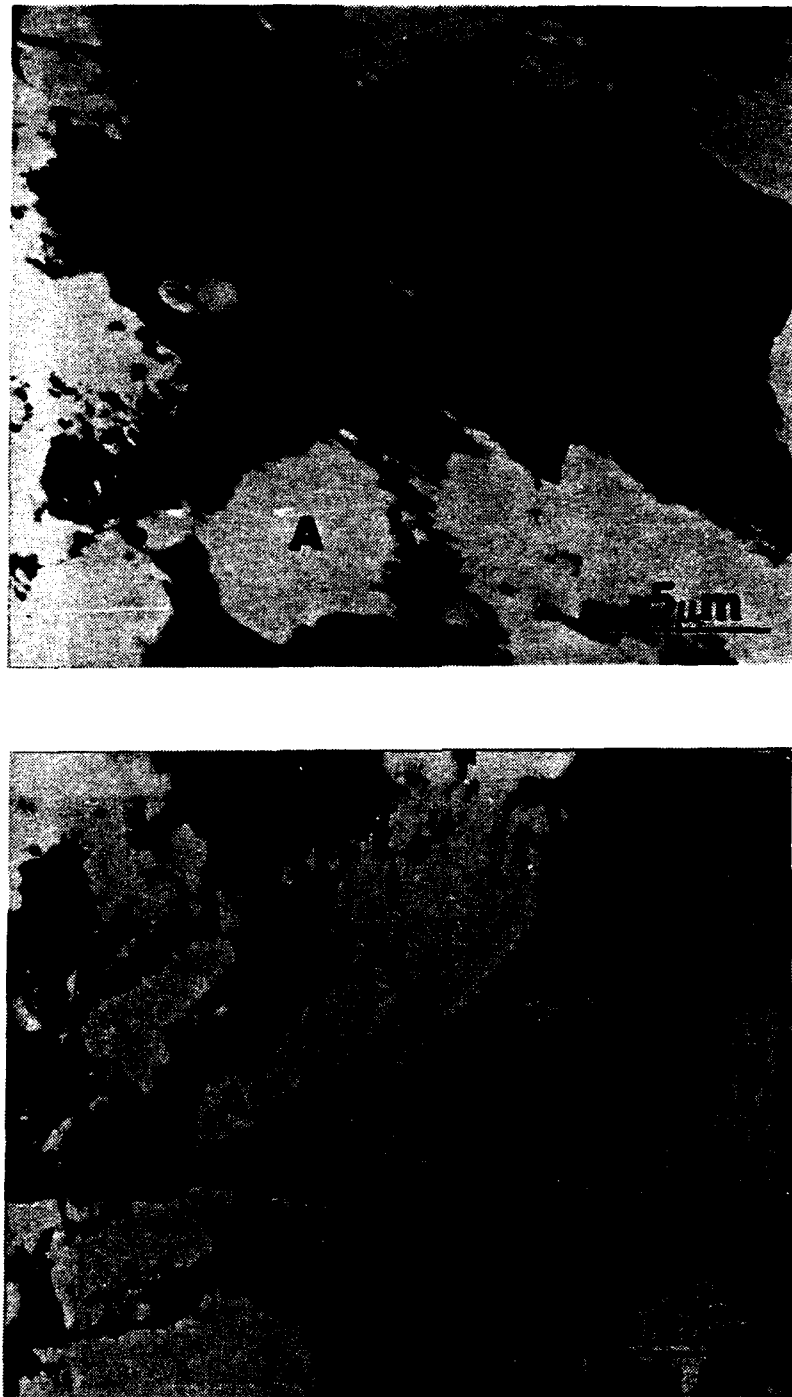


Figure 38. TEM Images of Bainite Lath and Ferrite Grain Structure in 677°C Aged HSLA-100 Steel: No SADP taken because of large number of grain orientations.



Figure 39. TEM Image of 677°C Aged HSLA-100 Steel Lath Structure

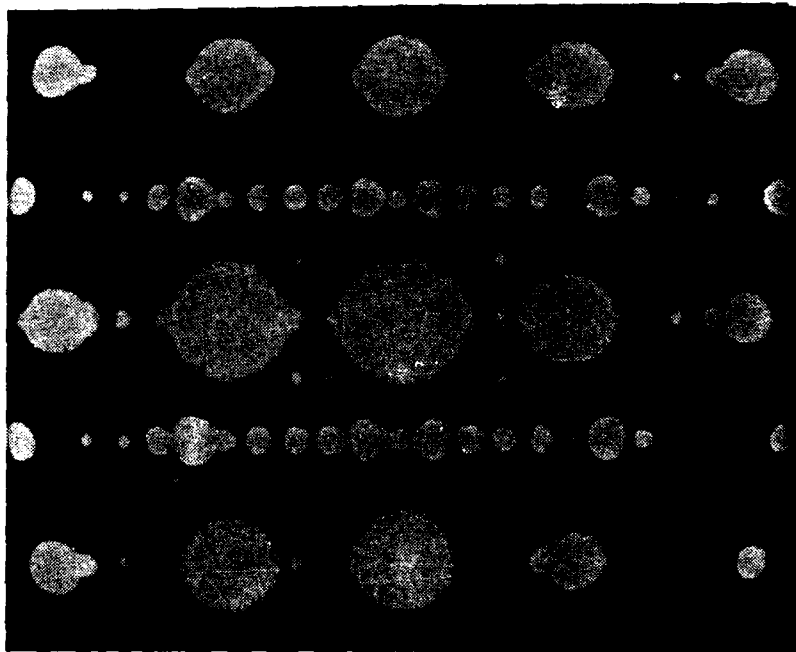


Figure 40. 677°C Aged HSLA-100 Steel SADP: \vec{B} close to $\langle 110 \rangle$, $\vec{g} = 110$ type.

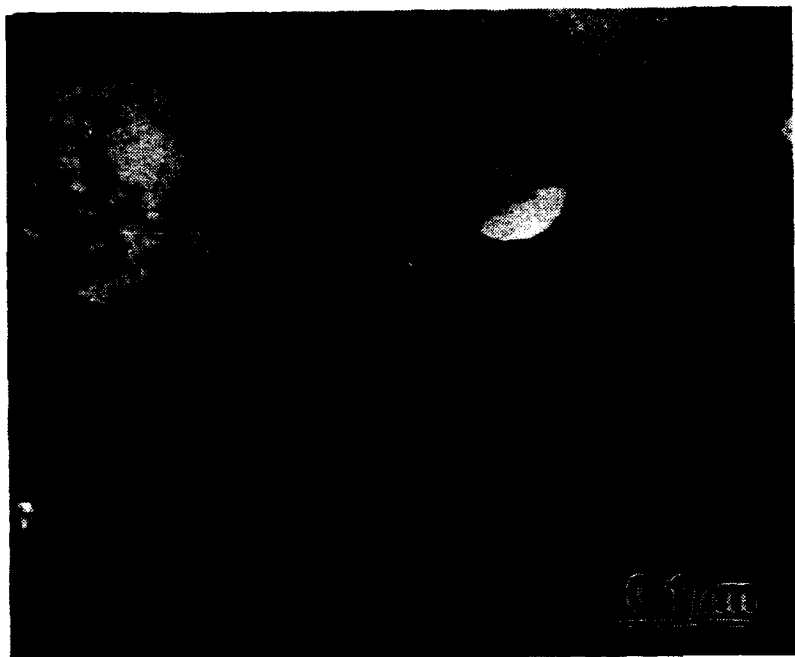


Figure 41. TEM Images of 677°C Aged HSLA-100 Steel Interlath and Intralath Carbides: Carbides too small to generate SADP.

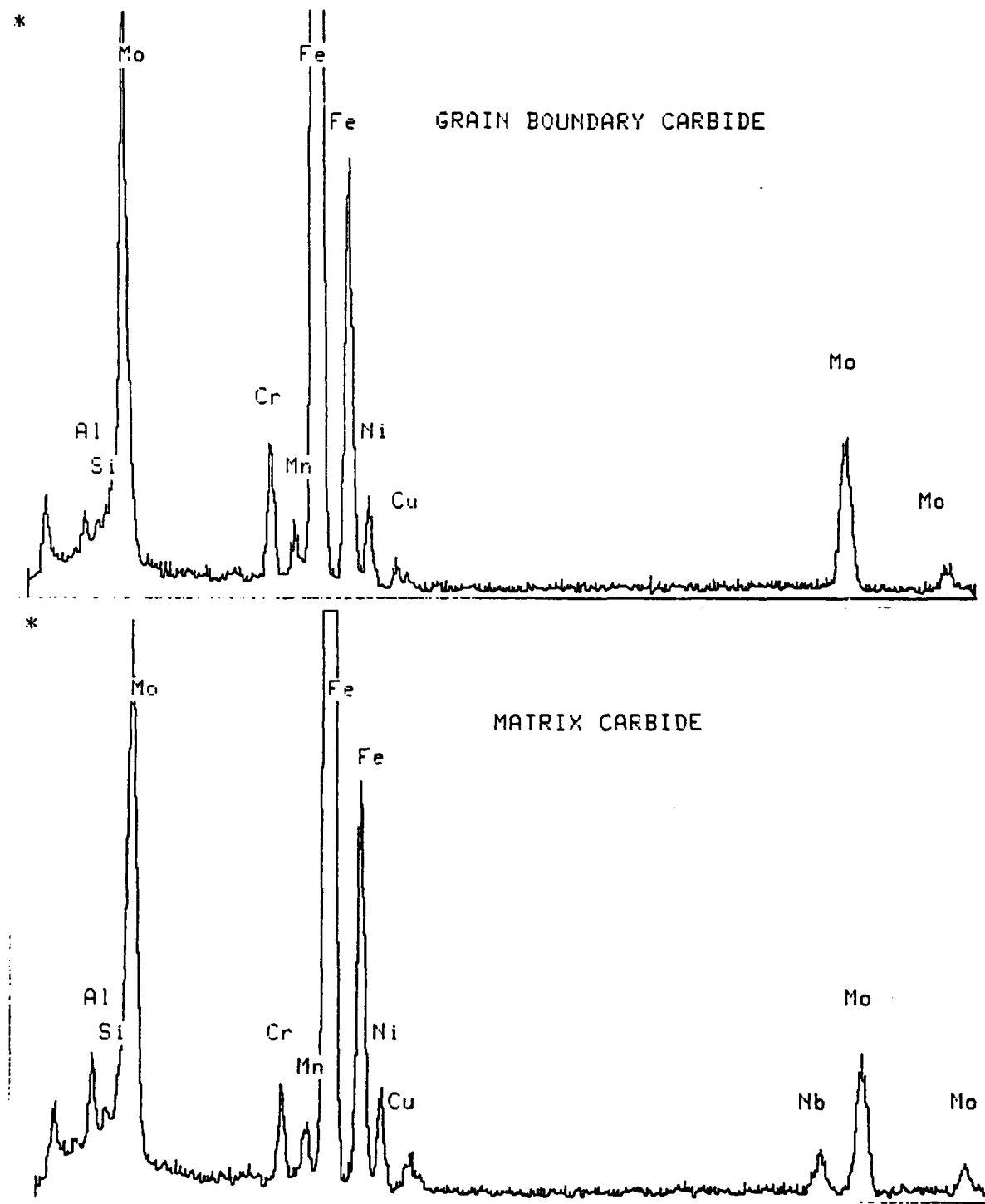


Figure 42. 677°C Aged HSLA-100 Steel Carbide EDX Spectra: (Top) Interlath carbide, (Bottom) Intralath carbide.



Figure 43. X-ray Mapping of 677°C Aged HSLA-100 Steel: (Top) Digitized map of area, (Middle) Molybdenum distribution, (Bottom) Copper distribution.

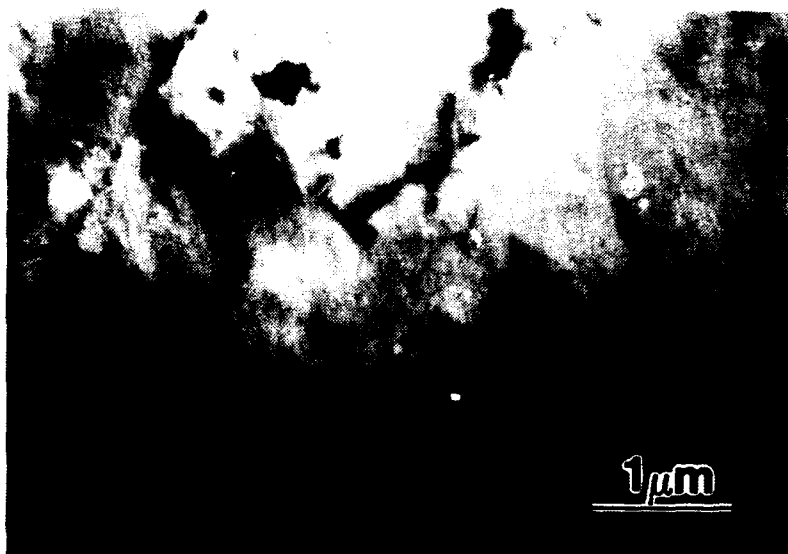


Figure 44. TEM Image of Lath Boundary Copper Precipitates in 677°C Aged HSLA-100 Steel: (Top) Bright field, (Bottom) Dark field. Micrographs taken well away from a low index pole to illuminate copper precipitates. Drift due to long exposure time required.

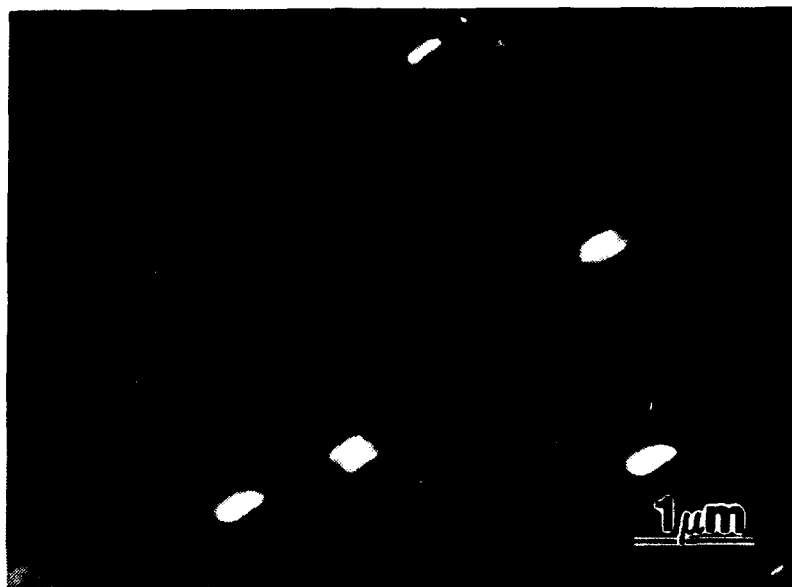
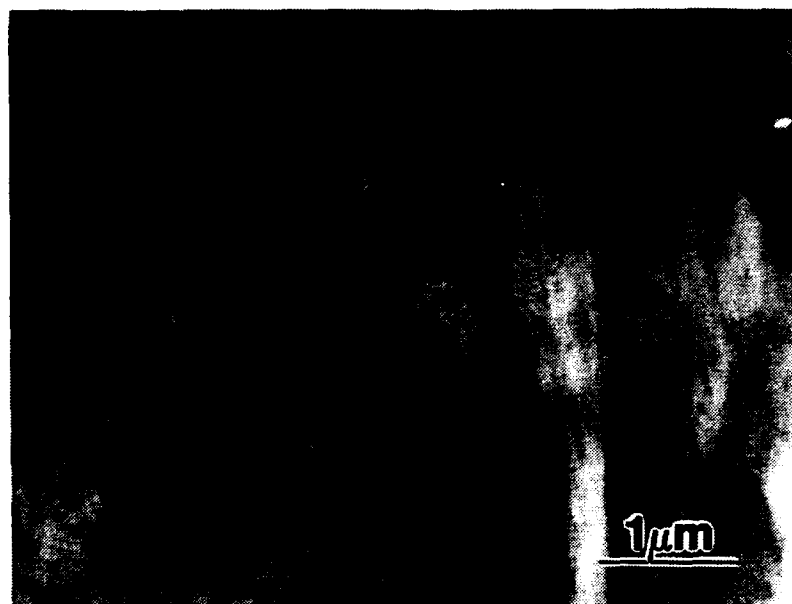


Figure 45. TEM Images of Interlath Copper Precipitates in 677°C Aged HSLA-100 Steel: (Top) Bright field, (Bottom) Dark field. Micrographs taken well away from a low index pole to illuminate copper precipitates. Drift due to long exposure time required.

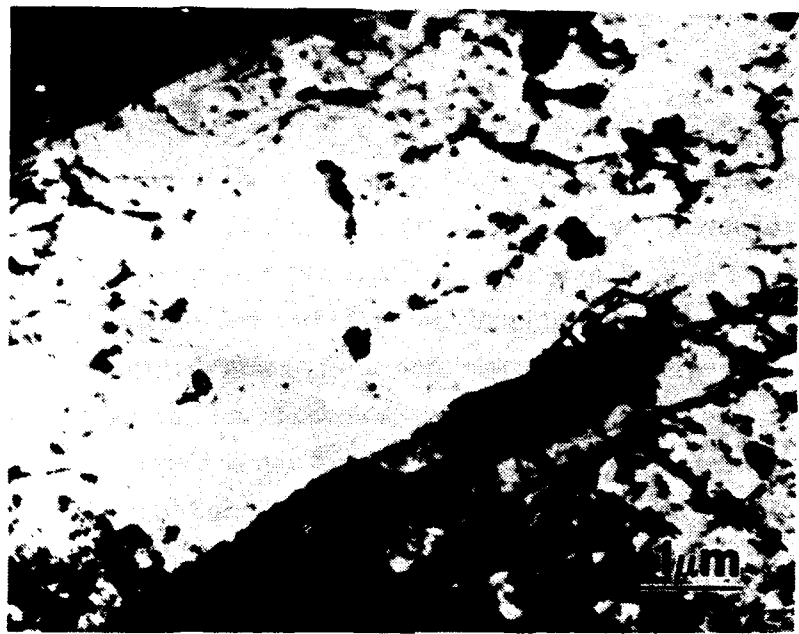


Figure 46. TEM Image of Copper Precipitates on Dislocations in 677°C Aged HSLA-100 Steel

V. DISCUSSION

The excellent strength and toughness properties of HSLA-100 steel are the result of the interaction of several mechanisms within the microstructure. The baseline properties are provided by the as-quenched material. The strength is primarily the result of the fine prior austenite grain size and the highly dislocated bainite substructure of the granular bainite microstructure. Both of these mechanisms increase the strength by impeding the motion of dislocations. Some strengthening is derived from the solid solution effects of alloying elements such as copper although, as discussed earlier, this effect is minimal at best. Nb- and Mo-carbides can provide a degree of precipitation strengthening if they precipitate during the quench although no conclusive evidence to this end was found. The toughness is the result of the fine prior austenite grain size. The high angle boundaries of the prior austenite grains serve to blunt the propagation of defects through the matrix, forcing the cracks to expend energy to reinitiate.

At the 454°C aging temperature, the peak strength is attained. Accompanying the peak strength is the minimum toughness of the steel. The strength and the toughness are controlled by the prior austenite grain size and by the precipitation of copper. The effect of the prior austenite grain size on both properties is essentially the same as it was in the as-quenched state since little grain growth has occurred. The bulk of the remaining strength is derived from the precipitation of fine coherent BCC copper clusters. The coherent copper precipitates create coherency strain fields which force the dislocations to bend in order to reach their low energy state. The coherency strain fields raise the stress required for a dislocation to move through the matrix thereby increasing the strength. While the interaction of the coherency strain fields and the dislocations raises the strength, the inability of the dislocations to move degrades the toughness. The copper clusters grow by bulk diffusion and are approximately 24Å in diameter at this temperature [Ref. 17] and are only about 50% copper [Ref. 18].

Carbide precipitates also play a role in the 454°C aged steel. The high strength of the carbides makes them essentially non-deformable such that they do not deform when a dislocation interacts with them. Dislocations are forced to bow around or loop the carbide. This increases the strength of the steel. The solid solutioning effect is reduced by the precipitation of the copper. Finally, the bainite dislocation substructure provides less strengthening due to the recovery of some of the dislocations.

When HSLA-100 steel is aged at temperatures above the peak aging temperature, the strength is reduced significantly while the toughness of the steel is recovered. One of the major factors contributing to this behavior is the growth of the copper precipitates. In the peak age condition, the copper precipitates are about 24\AA in diameter. As the steel is aged at overage aging temperatures, the copper precipitates exceed the peak strength size. At approximately 40\AA , the copper precipitates transform from coherent BCC to incoherent FCC [Ref. 18: p. 2377]. Strengthening by the overaged copper particles is the result of the interaction of dislocations with the overaged copper particles and arises from the difference in the elastic moduli of the overaged copper and the ferrite matrix [Ref. 21]. The growth of the particles increases the interparticle spacing which decreases the number of interactions between dislocations and the copper particles and, therefore, the strength decreases as the aging temperature increases. Grain size strengthening is degraded by the widening of the bainite laths, the slight increase in bainite packet size and the more equiaxed nature of the microstructure. Recovery of the bainite dislocation substructure is more pronounced at higher temperatures, reducing its effect on the strength of the steel. Finally, the solid solution strengthening effect is essentially nonexistent due to the precipitation of practically all the alloying elements that can. Not all factors contribute to the decline of the strength. The precipitated Nb- and Mo-carbides improve the strength by impeding the motion of the dislocations.

While the strength decreases in over-aged steel, the toughness increases. This is due to several factors. First, the incoherent ductile copper particles can act as crack arresters. The ductile copper particles absorb the energy of deformation by plastically deforming to blunt the crack tip. Secondly, significant recovery occurs, reducing the impact of the dislocation substructure and its associated energy. More energy must be put into the material in order for a crack to propagate. Finally, the fine distribution of the precipitated Nb- and Mo-carbides within the laths serve to deflect the cracks, forcing the cracks to expend energy to propagate around the carbides.

The strength and toughness of HSLA-100 steel at aging temperatures up through 566°C behave in a manner expected of typical copper age-hardened steels. The properties are controlled by the interaction of copper precipitates, prior austenite grain size effects, recovery of the bainite dislocation substructure and the precipitation of carbides.

At the 677°C aging temperature, significant changes occur in the HSLA-100 steel properties. The strength decreases at a much more rapid rate, the upper shelf impact energy experiences a significant increase and the DBTT drops considerably. The changes in the mechanical properties are the result of several factors. The first is the change of

the microstructure from granular bainite to a dual-phase mixture of bainitic ferrite laths, fine ferrite grain clusters and martensite. The dual-phase microstructure is the result of the recrystallization of the regions of high dislocation density into clusters of fine ferrite grains. The remaining areas of the bainitic ferrite laths grow in all directions. Recovery of the dislocations that do not recrystallize results in dislocation free bainitic ferrite laths. Retained austenite in the as-quenched state is transformed into martensite. This change of microstructure is the result of aging HSLA-100 steel at the lower transformation temperature. Examination of the iron-copper phase diagram, Figure 3, shows the eutectoid temperature at 850°C but this does not account for the impact of the alloying elements on the lower transformation temperature. The changes in the trends of the properties and of the microstructure indicate the eutectoid is lower. Research by Heinze, Coldren and Czyryca have placed the lower transformation temperature of HSLA-100 steel at approximately 677°C [Ref. 26: p. 50., Ref. 10: p. 626, Ref. 2: p. 6]. Thus aging at 677°C would put HSLA-100 steel in the bottom of the ferrite and austenite ($\alpha + \gamma$) region. Second, the diffusion of carbon from the retained austenite results in the precipitation of small 50-100Å carbides within the bainitic laths, 100-300Å carbides at dislocations and possibly prior austenite grain boundaries within the bainitic laths and large 500-1000Å carbides at bainite lath and ferrite grain boundaries. Finally, the copper precipitates are significantly overaged, appearing as 300-1000Å rod-like particles. The coarse copper particles, although uniformly distributed, are found in higher densities at bainite lath and ferrite grain boundaries.

The interaction of the dual-phase microstructure, the fine carbide distribution and the elastic moduli differences of the overaged copper particles and the ferrite matrix with dislocations provides the yield strength at a level comparable to that of the as-quenched steel. Dislocation motion is inhibited by the high-angle boundaries of the ferrite grains and the carbides. The lower elastic strength of the overaged copper particles, in relation to that of the ferrite matrix, inhibits the motion of the dislocations in a manner similar to Orowan strengthening but without the work hardening normally associated with Orowan looping.

The same elements of the HSLA-100 steel microstructure contribute to the toughness of the steel when aged at 677°C. The high-angle boundaries of the ferrite grains blunt crack motion. The fine carbides act as crack arresters, forcing the expenditure of more energy to reinitiate the crack. The ductile copper precipitates inhibit crack propagation by plastically deforming to blunt the crack tip. The combined effect of these mechanisms is to severely inhibit the propagation of cracks and increase the toughness.

VI. CONCLUSIONS

The excellent combination of strength and toughness properties of HSLA-100 steel appear to be the result of the interaction of a multitude of mechanisms within the microstructure. The microstructure and its effect on the properties was determined by the relation of the aging temperature to the lower transformation temperature, 677°C. Aging at temperatures below 677°C produced microstructures typical of copper age-hardened steels. The as-quenched steel had a granular bainite microstructure with islands of martensite and retained austenite. The peak aged steel, 454°C aging temperature, had a tempered bainite microstructure with coherent copper precipitates and evidence of carbide precipitation. The general microstructure did not change much in the 566°C aged steel from the peak aged steel with the exception of the copper precipitates transforming to incoherent spherical particles. The strength and toughness properties appear to be controlled primarily by grain size strengthening derived from the refined prior austenite grain size and by the precipitation of copper. Although not as significant as the grain size and the copper, the recovery of the bainite dislocation substructure and the precipitation of carbides contribute to the observed mechanical properties.

Aging at the lower transformation temperature produced significant differences in the mechanical properties and the microstructure. The microstructure had transformed from granular bainite to a dual-phase microstructure consisting of bainitic ferrite laths, clusters of fine ferrite grains and martensite with Nb- and Mo-carbides and overaged copper precipitates. Regions of high dislocation density had recrystallized to form clusters of fine ferrite grains. The fine ferrite grain and bainite lath size in conjunction with the fine carbide distribution and the elastic moduli strengthening appear to be the basis for the strength of the steel. The toughness is based on several factors. First, the high-angle boundaries of the ferrite grains blunt crack propagation. Second, the fine intralath carbides arrest crack motion and force the expenditure of more energy to reinitiate the crack. Finally, the ductile copper particles plastically deform to act as crack tip blunters. The combined effect of the strength and toughness mechanisms is to inhibit dislocation motion and crack propagation throughout the microstructure and enhance the strength and toughness of overaged HSLA-100 steel.

VII. RECOMMENDATIONS FOR FUTURE RESEARCH

Conduct a statistical analysis of the high-angle ferrite grain cluster distribution in the 677°C aged HSLA-100 steel and the bainite lath parameters for all aging variants of the steel to validate the distribution of the ferrite grain clusters in the 677°C aged steel and the bainite lath growth with respect to aging temperature. Study of the ferrite grain cluster distribution and the bainite lath parameters would provide a better understanding of the phase transformation that occurs at 677°C and would seem to be the key to the high fracture toughness exhibited by HSLA-100 steel when aged at 677°C.

Conduct an investigation of the size, chemical composition and distribution of the carbide precipitates including the use of extensive X-ray mapping and statistical analysis. This would provide a better understanding of the role of precipitated carbides in the strength and toughness mechanisms at work in the HSLA-100 steel microstructure.

Pursue a more efficient manner of thinning the HSLA-100 steel TEM samples such that they may be used for tilting experiments in the TEM without severe magnetic distortion problems in order to allow advanced crystallographic analysis of the HSLA-100 steel microstructure. This would provide a better understanding of the relationship between the ferrite matrix and the alloying elements such as carbon, copper, niobium and molybdenum and the microstructural constituents such as martensite and retained austenite and thereby lead to an improved understanding of the roles these components play in the development of the mechanical properties of HSLA-100 steel.

LIST OF REFERENCES

1. Wilson, Alexander D., *High Strength, Weldable Precipitation Aged Steels*, Journal of Metals, March 1987, pp. 36-38.
2. Czyryca, Ernest J., *Development of Low-Carbon, Copper-Strengthened HSLA Steel Plate for Naval Ship Construction*, DTRC-SME-90/21, June 1990.
3. Montemarano, T.W., B.P. Sack, J.P. Gudas, M.G. Vassilaros and H.H. Vanderveldt, *High Strength Low Alloy Steels in Naval Construction*, Journal of Ship Production, Vol. 2, No. 3, August 1986, pp. 145-162.
4. Czyryca, Ernest J., R.E. Link, R.J. Wong, D.A. Aylor, T.W. Montemarano and J.P. Gudas PHD, *Development and Certification of HSLA-100 Steel for Naval Ship Construction*, Naval Engineers Journal, May 1990, pp. 63-82.
5. Coldren, A.P. and T.B. Cox, *Development of 100 KSI Yield Strength HSLA Steel*, DTNSRDC/SME-CR-07-86, July 1986.
6. Cohen, M. and S.S. Hansen, *On The Fundamentals of HSLA Steels*, HSLA Steels: Metallurgy and Applications, Proceedings of an International Conference on HSLA Steels '85, ASM International, 1985.
7. Abrams, H. and others, *Production Technology of Bethlehem's HSLA Plate Steels - Past, Present and Future*, HSLA Steels: Metallurgy and Applications. Proceedings of an International Conference on HSLA Steels '85, Edited by J.M. Gray and others, ASM International, 1985.
8. Hertzberg, R.W., *Deformation and Fracture Mechanics of Engineering Materials*, 3d ed., John Wiley & Sons, Inc., 1989.
9. Pickering, F.B., *Physical Metallurgy and the Design of Steels*, Applied Science Publishers LTD, London, 1978.

10. Wilson, A.D. and others, *Properties and Microstructures of Copper Precipitation Aged Plate Steels*, Microalloyed HSLA Steels, Proceedings of Microalloying '88, ASM International, 1988.
11. Le May, I. and L. McDonald Schekty, *Copper in Iron and Steel*, John Wiley and Sons, New York, 1982.
12. Le May, I., L. McD. Schetky, and M.R. Krishnadev, *The Role of Copper in HSLA Steels: A Review and Update*, High Strength Low Alloy Steels, Ed. by D.P. Dunne and T. Chandra, 1984.
13. Czyryca, E.J. and R.E. Link, *Physical Properties, Elastic Constants, and Metallurgy of HSLA-100 Steel Plate*, DTRC/SME-88/62, December 1988.
14. Honeycombe, R.W.K., *Fundamental Aspects of Precipitation in Microalloyed Steels*, HSLA Steels: Metallurgy and Applications, Proceedings of an International Conference on HSLA Steels '85, ASM International, 1985.
15. Hornbogen, E. and R.C. Glenn, *A Metallographic study of Precipitation of Copper from Alpha Iron*, Transactions of the Metallurgical Society of AIME, Vol. 218, December 1960, p. 1064.
16. Hornbogen, E., *Aging and Plastic Deformation of an Fe-0.9% Cu Alloy*. Transactions of the ASM, Vol. 57, 1964, p.120.
17. Goodman, S.R., S.S. Brenner, and J.R. Low, *An FIM-Atom Probe Study of the Precipitation of Copper from Iron-1.4 At. Pct Copper. Part I: Field-Ion Microscopy*. Metallurgical Transactions, Vol. 4, October 1973, p. 2363.
18. Goodman, S.R., S.S. Brenner, and J.R. Low, *An FIM-Atom Probe Study of the Precipitation of Copper from Iron-1.4 At. Pct Copper. Part II: Atom Probe Analysis*. Metallurgical Transactions, Vol. 4, October 1973, p. 2371.

19. Dhamen, U., P. Ferguson, and K.H. Westmacott, *Invariant Line Strain and Needle-Precipitate Growth Direction in Fe-Cu*, *Acta Metallurgica*, Vol. 32, No. 5, 1984, pp. 803-810.
20. Speich, G.R. and R.A. Orani, *The Rate of Coarsening of Copper Precipitate in an Alpha-Iron Matrix*, *Transactions of the Metallurgical Society of AIME*, Vol. 233, April 1965, p. 623.
21. Russell, K.C. and L.M. Brown, *A Dispersion Strengthening Model Based on Differing Elastic Moduli Applied to the Iron-Copper System*, *Acta Metallurgica*, Vol. 20, July 1972, p. 969.
22. Howell, P.R., *Microstructural Development in HSLA-100 Steel Weld Metals*, paper received from author at David Taylor Research Center meeting on HSLA-100 Steel, 15 October, 1990.
23. Bucher, J.H., E.G. Hamburg, and A.D. Wilson, *Comments on High-Strength Steels Produced by Advanced Metallurgical Processes*, by I.L. Stern and others, *Journal of Ship Production*, Vol 4, No. 3, August 1988, pp. 182-4.
24. Hamburg, E.G. and A.D. Wilson, *Production and Properties of Copper, Age Hardened Steels*, *Processing, Microstructure and Properties of HSLA Steels*, edited by A.J.DeArdo, The Minerals, Metals & Materials Society, 1988.
25. Mikalac, S., (DTRC Code 2814) letter to Dr. Alan G. Fox, Subject: Thermo-mechanical Processing of Lot GQH HSLA-100 Steel, 9 NOV 1990.
26. Heinze, M.H., *The Effect of Aging Treatment on the Microstructural and Properties of Copper-Precipitation Strengthened HSLA Steel*, Master's Thesis, Naval Post-graduate School, Monterey, California, December 1988.
27. Miglin, M.T. and others, *Microstructure of a Quenched and Tempered Cu-Bearing High-Strength Low-Alloy Steel*, *Metallurgical Transactions A*, Vol. 17a, May 1986, pp. 791-8.

INITIAL DISTRIBUTION LIST

	No. Copies
1. Defense Technical Information Center Cameron Station Alexandria, VA 22304-6145	2
2. Library, Code 52 Naval Postgraduate School Monterey, CA 93943-5002	2
3. Department Chairman, Code MEHy Department of Mechanical Engineering Naval Postgraduate School Monterey, CA 93943-5000	1
4. Naval Engineering Curricular Office, Code 34 Naval Postgraduate School Monterey, CA 93943-5000	1
5. Professor A.G. Fox, Code MEFx Department of Mechanical Engineering Naval Postgraduate School Monterey, CA 93943-5000	2
6. Mr. E.J. Czyryca, Code 2814 David Taylor Research Center Annapolis, MD 21402	1
7. Dr. M.G. Vassilaros, Code 2814 David Taylor Research Center Annapolis, MD 21402	1
8. Ms. Stephanie Mickalac, Code 2814 David Taylor Research Center Annapolis, MD 21402	1
9. Mr. C.J. Echer National Center for Electron Microscopy Lawrence Berkeley Laboratory, Bldg. 72 University of California Berkeley, CA 94720	1
10. LT Victor R. Mattes, USN 6018 South 74th East Avenue Tulsa, OK 74145	3